ISSN 2531-2189

Volume 7, Issue 19 — January — June — 2023

Journal of Mechanical Engineering

ECORFAN®

Journal of Mechanical Engineering, Volume 7, Number 19, June - 2023, is a biannually Journal edited by ECORFAN-Spain. Matacerquillas Street 38, CP: 28411. Moralzarzal - Madrid. WEB: http://www.ecorfan.org/spain/rj_ingenieria_mec.php, revista@ecorfan.org. Editor in Chief: SERRUDO-GONZALES, Javier, BsC. ISSN 2531-2189. Responsible for the last update of this issue ECORFAN Computer Unit. Imelda Escamilla Bouchán, PhD. Vladimir Luna Soto, PhD. Updated as of June 30, 2023.

Journal of Mechanical Engineering

Definition of Journal

Scientific Objectives

Support the International Scientific Community in its written production of Science, Innovation Technology in the Area of Engineering and Technology, in the Subdisciplines of pumps and equipment for handling liquids, bearings, air compressors, gears, refrigeration equipment, mechanical power transmission equipment, pneumatic equipment, equipment and industrial machinery, agricultural machinery, oil extraction machinery, printing and reproduction machinery , Mining Machinery, Hydraulic Machinery, Specialized Industrial Machinery, Nuclear Machinery, Paper Manufacturing Machinery, Machinery for the Food Industry, Material Handling Machinery, Textile Machinery, Steam Machinery, Vending and Distributor Machines, Machines, Tools and Accessories, Heating Material, Construction Material, Dies, Insoles and Gauges, Internal Combustion Engines (General), Gas Engines, Machined Operations.

ECORFAN-Mexico SC is a Scientific and Technological Company in contribution to the Human Resource training focused on the continuity in the critical analysis of International Research and is attached to CONAHCYT-RENIECYT number 1702902, its commitment is to disseminate research and contributions of the International Scientific Community, academic institutions, agencies and entities of the public and private sectors and contribute to the linking of researchers who carry out scientific activities, technological developments and training of specialized human resources with governments, companies and social organizations.

Encourage the interlocution of the International Scientific Community with other Study Centers in Mexico and abroad and promote a wide incorporation of academics, specialists and researchers to the publication in Science Structures of Autonomous Universities - State Public Universities - Federal IES - Polytechnic Universities - Technological Universities - Federal Technological Institutes - Normal Schools - Decentralized Technological Institutes - Intercultural Universities - S & T Councils - CONAHCYT Research Centers.

Scope, Coverage and Audience

Journal of Mechanical Engineering is a Journal edited by ECORFAN-México S.C in its Holding with repository in Spain, is a scientific publication arbitrated and indexed on a quarterly basis. It supports a wide range of contents that are evaluated by academic pairs by the Double-Blind method, around topics related to the theory and practice of pumps and equipment for handling liquids, bearings, air compressors, gears, cooling equipment, mechanical power transmission equipment, pneumatic equipment, equipment and industrial machinery, agricultural machinery, oil extraction machinery , printing and reproduction machinery, mining machinery, hydraulic machinery, specialized industrial machinery, nuclear machinery, paper manufacturing machinery, machinery for the food industry, material handling machinery, textile machinery, steam machinery, vending machines and distributors, machines, tools and accessories, heating material, building material, dies, insoles and gauges, internal (general) combustion engines, gas engines , mechanized operations with diverse approaches and perspectives, which contribute to the dissemination of the development of Science Technology and Innovation that allow arguments related to decision-making and influence the formulation of international policies in the Field of Engineering and Technology Sciences. The editorial horizon of ECORFAN-Mexico® extends beyond the academy and integrates other research and analysis segments outside this field, as long as they meet the requirements of argumentative and scientific rigor, as well as addressing topics of general and current interest of the International Scientific Society.

Editorial Board

Arbitration Committee

Assignment of Rights

The sending of an Article to Journal of Mechanical Engineering emanates the commitment of the author not to submit it simultaneously to the consideration of other series publications for it must complement the Originality Format for its Article.

The authors sign the Authorization Format for their Article to be disseminated by means that ECORFAN-Mexico, S.C. In its Holding Spain considers pertinent for disclosure and diffusion of its Article its Rights of Work.

Declaration of Authorship

Indicate the Name of Author and Coauthors at most in the participation of the Article and indicate in extensive the Institutional Affiliation indicating the Department.

Identify the Name of Author and Coauthors at most with the CVU Scholarship Number-PNPC or SNI-CONAHCYT- Indicating the Researcher Level and their Google Scholar Profile to verify their Citation Level and H index.

Identify the Name of Author and Coauthors at most in the Science and Technology Profiles widely accepted by the International Scientific Community ORC ID - Researcher ID Thomson - arXiv Author ID - PubMed Author ID - Open ID respectively.

Indicate the contact for correspondence to the Author (Mail and Telephone) and indicate the Researcher who contributes as the first Author of the Article.

Plagiarism Detection

All Articles will be tested by plagiarism software PLAGSCAN if a plagiarism level is detected Positive will not be sent to arbitration and will be rescinded of the reception of the Article notifying the Authors responsible, claiming that academic plagiarism is criminalized in the Penal Code.

Arbitration Process

All Articles will be evaluated by academic peers by the Double Blind method, the Arbitration Approval is a requirement for the Editorial Board to make a final decision that will be final in all cases. MARVID® is a derivative brand of ECORFAN® specialized in providing the expert evaluators all of them with Doctorate degree and distinction of International Researchers in the respective Councils of Science and Technology the counterpart of CONAHCYT for the chapters of America-Europe-Asia- Africa and Oceania. The identification of the authorship should only appear on a first removable page, in order to ensure that the Arbitration process is anonymous and covers the following stages: Identification of the Journal with its author occupation rate - Identification of Authors and Coauthors - Detection of plagiarism PLAGSCAN - Review of Formats of Authorization and Originality-Allocation to the Editorial Board-Allocation of the pair of Expert Arbitrators-Notification of Arbitration -Declaration of observations to the Author-Verification of Article Modified for Editing-Publication.

Instructions for Scientific, Technological and Innovation Publication

Knowledge Area

Work should be unpublished and refer to issues of Pumps and equipment for handling liquids, bearings, air compressors, gears, cooling equipment, mechanical power transmission equipment, pneumatic equipment, equipment and industrial machinery, agricultural machinery, oil extraction machinery, printing and reproduction machinery, mining machinery, hydraulic machinery, specialized industrial machinery, nuclear machinery, machinery to manufacture paper , machinery for the food industry, material handling machinery, textile machinery, steam machinery, vending machines and distributors, machines, tools and accessories, heating material, building material, dies, insoles and gauges, internal combustion engines (general), gas engines, machined operations and other topics related to engineering and technology sciences.

Presentation of Content

In volume five, issue fifteen, as the first article we present, *Dimensional Analysis of thickness of strip for a four high cold mill*, by DIAZ-SALINAS, Juan Andrés, SERVIN-CASTAÑEDA, Rumualdo, ARREOLA-VILLA, Sixtos Antonio and PEREZ-ALVARADO, Alejandro, with secondment at the Universidad Autónoma de Coahuila, as a second article we present, *Fuzzy Modeling of DC Motors using the stimulus-response method*, by GONZÁLEZ-CASTOLO, Juan Carlos, RAMOS-CABRAL, Silvia, HERNÁNDEZ-RUEDA, Karen and ZATARAIN-DURÁN, Omar Alí, with an appointment at Universidad de Guadalajara, as a third article we present, *Numerical and experimental analysis of the bodywork of a Formula SAE 2023 type vehicle*, by HERNANDEZ-URBANO, Cesar, CORDERO-GURIDI, José de Jesús, NOCHEBUENA-TIRADO, Carlos Jordán and VILLARREAL-CHAPA, José Ángel, with secondment at the Universidad Popular Autónoma del Estado de Puebla, as fourth article we present, *Comparison of microstructure and mechanical properties of industrial pure aluminum produced by powder metallurgy and conventional rolling*, by SALGADO-LÓPEZ, Juan Manuel, MARTINEZ-FRANCO, Enrique, CRUZ-GONZÁLEZ, Celso Eduardo and TELLO-RICO, Mauricio, with secondment Centro de Ingeniería y Desarrollo Industrial CIDESI.

Content

Article **Journal of Mechanical Engineering**
June, 2023 Vol.7 No.19 1-5

Dimensional Analysis of thickness of strip for a four high cold mill

Análisis dimensional del espesor de la lámina para un castillo de laminación en frio cuatro alturas

DIAZ-SALINAS, Juan Andres†[1], SERVIN-CASTAÑEDA, Rumualdo*[2], ARREOLA-VILLA, Sixtos Antonio[2] and PEREZ-ALVARADO, Alejandro[2]

[1]*Doctorado en Ciencias – UAdeC, Centro Cultural 2º. Piso. Ciudad Universitaria, Carretera México Km 13, C.P 25350 Arteaga Coahuila, México*
[2]*Facultad de Ingeniería Mecánica y Eléctrica – UAdeC. Barranquilla S/N, Colonia Guadalupe, C.P 257500 Monclova Coahuila. México*

ID 1st Author *Juan Andres, Diaz-Salinas* / **ORC ID**: 0009-0009-0706-2355

ID 1st Co-author *Rumualdo, Servin-Castañeda* / **ORC ID**: 0000-0002-8655-2572

ID 2nd Co-author: *Sixtos Antonio, Arreola-Villa* / **ORC ID**: 0000-0002-6348-0860

ID 3rd Co-author: *Alejandro, Perez-Alvarado* / **ORC ID**: 0000-0003-0420-5153

DOI: 10.35429/JME.2023.19.7.1.5 Received: March 30, 2023; Accepted: May 30, 2023

Abstract

In the present study, a Finite Element Method (FEM)is used to model in 3D and simulation of a cold rolling mill Four High, to analyze flatness, geometry and thickness of rolling strip when constant variables of rolling force, materials properties, dimensions of rolls and strip; considering +0.03937mm of constant positive crown on Back Up Roll and combinations of +0.1016mm, +0.254mm y +0.508mm on Work Roll, The results shown that there is a instability zone of 76mm for all the analyzed cases in the end of the strip, this geometry is symmetrical in both ends of the strip. When the crown of work rolls is increase, the instability zone starts to move toward to the middle of the strip. With the increase of crown from +0.03937mm to +0.508mm the generated strain is only 0.020 mm, and we can see that strain is bigger in the middle of strip.

Strip, Flatness, Pressure

Resumen

El presente estudio se realiza utilizando un Método de Elementos Finitos para modelado en 3D y simulación de un molino de laminación en frio Four High, para analizar la planeza, forma y espesor de la lámina rolada cuando se utilizan variables fijas de fuerzas de rolado, propiedades de los materiales, dimensiones de los rodillos y la lámina rolada; considerando constante la corona positiva de +0.03937mm en los rodillos de apoyo y combinaciones de +0.1016mm, +0.254mm y +0.508mm en los rodillos de trabajo. Los resultados muestran que hay una zona de inestabilidad de 76mm para todos los casos en el extremo de la lámina, esta geometría es simétrica en los dos extremos de la lámina. Cuando la corona de los rodillos de trabajo se incrementa, la zona de inestabilidad comienza a moverse hacia el centro de la lámina. Con el incremento de corona de +0.03937mm a +0.508mm la deformación generada es de tan solo 0.020 mm, y se puede observar que la deformación es mayor en el centro de la lámina.

Lamina, Planeza, Presión

Citation: DIAZ-SALINAS, Juan Andres, SERVIN-CASTAÑEDA, Rumualdo, ARREOLA-VILLA, Sixtos Antonio and PEREZ-ALVARADO, Alejandro. Journal of Mechanical Engineering. 2023. 7-19: 1-5

† Researcher contributing as first author.

Introduction

Steel is one of the most important materials in the development of the current economy, it can be recycled without losing its mechanical properties, it is a sustainable material that makes it the most recycled material.

Consequently, steel is one of the most important materials in the world, due to its multiple uses it is considered the pillar of technological development in the economy.

Once the steel is produced, one of the most used mechanical forming processes is the rolling process, in which rolling mills are used to shape the products.

For this process there are many variables that must be considered, always keeping in mind considering the surface quality of the strip. Yan-Lin Li and Jian-Guo Cao (2015), developed a mathematical model where they consider the main variables of the rolling process with thermal crowns and wear of the rolls, Zhang Guo-min and Xiao Hong (2006) also developed a three-dimensional model, considering the same operating variables to study the pressure distribution between the rolls and the rolling strip.

Other scientists such as Guang-ming Liu et al (2018), have studied the effect of roll geometry due to axial forces and more specifically *Guanghui Yang* et al (2008), Xianodong Wang et al (2012) and Ning Kong et al. al (2014) have studied the contour of the Back Up rolls seeking to optimize the pressure distribution between the Back Up Roll (BUR) and Work Rolls (WR), using Smart Crown or Continuous Variable Crown (CVC), looking for uniform pressure on the strip and develop a Finite Element Method (FEM) for systematic control for the shape and flatness of the strip as proposed by Li Hai-jun et al (2010) and Liu Xiang-hua et al (2008), and even validate data at industrial scale such as those shown in the technological development of Cao, J.et al (2008).

When there is no control in the rolling variables, it results in inadequate surface quality of the strip, obtaining products with dimensional differences due to the inadequate distribution of rolling forces; the use of FEM are indispensable tools for the technological development of rolling processes, the present study is a tool that allows predicting what the results would be if the crowns of the work rolls are varied.

Research Methodology

The present study consists of the analysis of pressure distribution and stresses that generate the deformation of the strip, applied to the cold rolling process for a Four High rolling mill, for which a FEM developed by Rumualdo Servin et al (2019), considering constant the main variables and conditions of the rolling process shown in Figure 1, and the parameters are specified in Table 1.

For the cases of analysis, the crown of the BUR is considered constant, which is 0.03937mm, and variable crowns of the work rolls, for which the following combinations are analyzed:

a) BUR0.03937mm-WR0.1016mm
b) BUR0.03937mm-WR0.254mm
c) BUR0.03937mm-WR0.508mm

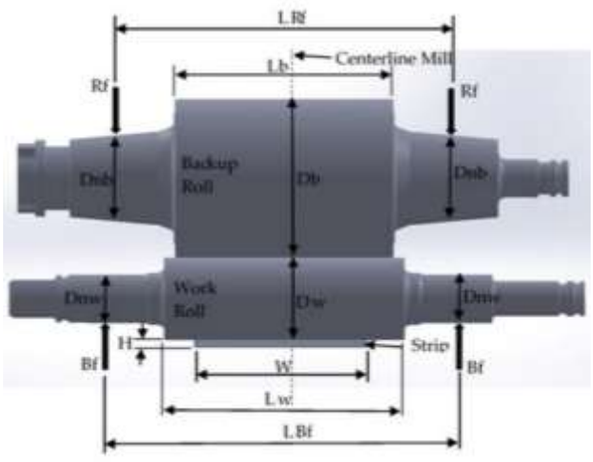

Figure 1 Representation of the main rolling variables

Model Parameter	Value
Work roll diameter Dw	356.870 mm
Work roll barrel length Lw	838.200 mm
Work roll neck diameter Dnw	206.197 mm
Work roll Bending force length LBf	1428.750 mm
Backup roll diameter Db	812.800 mm
Backup roll barrel length Lb	857.250 mm
Backup roll neck diameter Dnb	479.221 mm
Backup roll Rolling force length LRf	1676.400 mm
Strip width W	520.700mm
Strip thickness H	6.096mm
Rolling force Rf	4,893 kN
Piosson´s ratio work roll	0.29
Poisson´s ratio backup roll	0.29
Young´s modulus work roll	200 Gpa
Young´s modulus backup roll	200 Gpa
Work Roll Crown	0.1016mm, 0.254mm and 0.508mm
Backup Roll Crown	0.03937mm
Young´s modulus strip	205 MPa
Maximum Thermal crown WR	0.150 mm
Maximum Thermal crown BUR	0.100 mm
Maximum wear WR	0.150 mm
Maximum wear BUR	0.600 mm
Chamfer of BUR	76.200mm x 6.604 mm
Chamfer of WR	No Taper

Table 1 Values for the parameters considered

The results were validated at industrial scale, obtaining similar results with a margin of error of ±10%. Figure 2, shows the illustration of the simulated model, the rolling forces are uniformly distributed and applied in the bearing area, as shown in the figure in the areas in red; elastic deformation is considered for the rolls and the strip, using a model with a linear relationship between stress and deformation, the arrangement of the model allows vertical movement in the direction of the applied force.

The mesh is generated using smart meshing, defined by nodes and has three degrees of freedom per node, which are translation in X, Y and Z directions.

The mesh in the contact regions was refined, it is guaranteed that the zones are always in contact, there is no possibility of separation between the surfaces and the model was implemented without penetration.

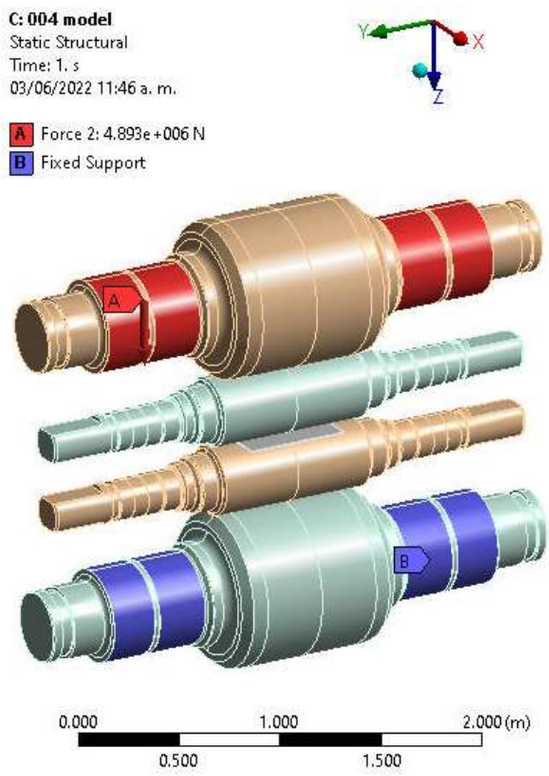

Figure 2 Graphic representation of the 3D model

Results

Figure 3 illustratively shows the stress values for crown combinations a), b) and c) respectively. Where it can be seen that the maximum stress values are 300 MPa and are located in two contact zones, the first contact zone is between the BUR and WR and the second is between the strip and the work roll; our case study is focused on analyzing only the contact area between the strip and the work roll, where we can see that for the three cases there are stress concentration points, however, for combination c), the stress tends to be concentrated in a punctual way in the center of the strip.

ISSN-2531-2189

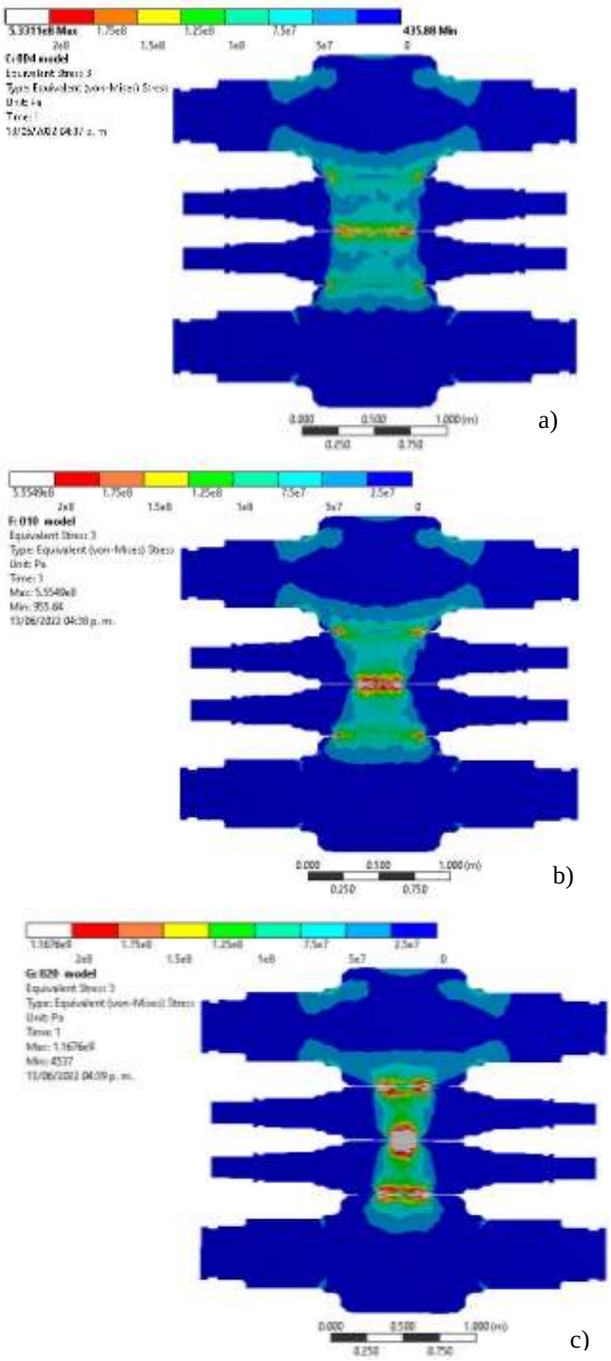

Figure 3 Illustrative representation of the stress for the crown combinations a) BUR0.03937mm-WR0.1016mm b) BUR0.03937mm-WR0.254mm and c) BUR0.03937mm-WR0.508mm

Figure 4 illustratively shows the deformation values, where it can be seen that for combination a), the greatest deformation is concentrated at the ends of the strip, approximately 76 mm wide; for combination b) the deformation tends to move towards the center of the strip and reaches values of 0.005mm and finally for combination c) the greatest deformation is found in the center of the strip, reaching values of 0.020 mm.

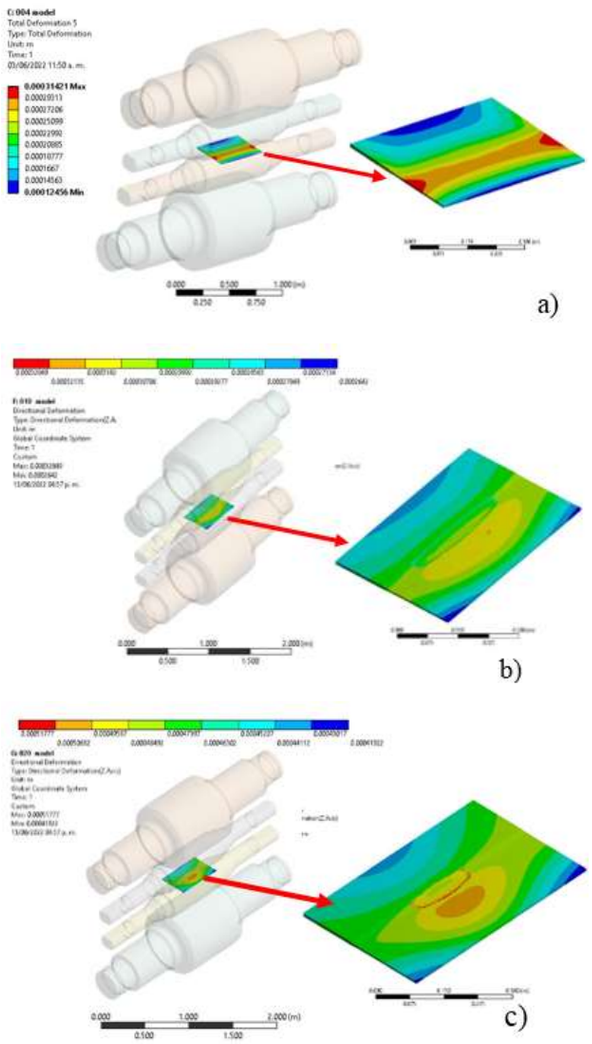

Figure 4 Illustrative representation of the deformation for the crown combinations a), b) and c)

For a better analysis of the deformations obtained, the graphs of Figure 5 were constructed, where it can be observed that the simulated deformation tends to concentrate in the center of the strip as the crown of the work rolls increases, for this case in particular for the 0.254mm crown it varies from 6.090mm to 6.095mm and for the 0.508mm crown it varies from 6.076mm to 6.096mm.

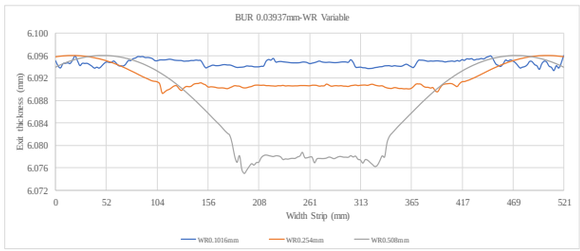

Figure 5 Graphs of simulated deformation, for the different types of crowns in WR and constant crown in BUR

Conclusions

For all three cases the same performance behavior is observed, the maximum stress concentration is located in two zones, BUR and WR contact zone and WR and strip contact zone; for the case of WR and strip contact zone the stress produces the deformation of the strip due to difference of mechanical properties of the strip, in others words, it is due to the WR is harder than the strip.

There is a stress concentration zone of 76mm wide approximately in the end of strip, it is symmetrical on both sides. When the Crown is increased in WR the stress concentration zone starts to move towards the middle of the strip. The width of 76mm is maintained moreover the direction of deformation changes. The phenomenon continues being symmetrical on both sides.

With the modification of positive Crown on WR from 0.1016mm to 0.508mm, the maximum deformation generated on the strip is only 0.020mm, moreover, it is considerable for the dimensional quality of the strip.

The stress concentration indicates instability of distribution of pressure and consequently alterations on the flatness and thickness of the strip, such as shown in the above images and graphics. There is a relationship between the Stress and deformation of the strip, and consequently it is due to the pression distribution along the width of the strip.

References

Cao, J.; Wei, G.; Zhang, J.; Chen, X.; Zhou, Y. VCR and ASR technology for profile and flatness control in hot strip mills. *J. Cent. South. Univ. Technol.* 2008, *15*, 264–270. http://dx.doi.org/10.1007/s11771-008-0049-0

Guanghui Yang, Jianguo Cao. Backup roll contour of a Smart Crown tandem cold rolling mill. *Journal of University of Science and Technology Beijing, Materials, 2008, 357-361* https://doi.org/10.1016/S1005-8850(08)60067-5

Guang-ming Liu, Yu-gui Li. Axial Force Analysis and Roll Contour Configuration of Four-High CVC Mill. Mathematical Problems in Engineering, 2018, 1-12. https://doi.org/10.1155/2018/7527402

Li Hai-jun, Xu Jian-zhong. Development of Strip Flatness and Crown Control Model for Hot Strip Mills. Journal of Iron and Steel Research International, 2010, 21-27. https://doi.org/10.1016/S1006-706X(10)60067-2

Liu Xiang-hua, SHI Xu. FEM Analysis of Rolling Pressure Along Strip Width in Cold Rolling Process. Journal of Iron and Steel Research International, 2007, 22-26. https://doi.org/10.1016/S1006-706X(07)60068-5

Ning Kong, Jianguo Cao. Development of Smart Contact Backup Rolls in Ultrawide Stainless Strip Rolling Process. Materials and Manufacturing Processes, 2014, 129-133. https://doi.org/10.1080/10426914.2013.822979

Rumualdo Servin, Sixtos A. Arreola, Ismael Calderón, Alejandro Perez and Sandra M. San Miguel. Effect of Crown Shape of Rolls on the Distribution of Stress and Elastic Deformation for Rolling Processes, **Metals** 2019, **9**(11), 1222. https://doi.org/10.3390/met9111222

Xiaodong Wang, Fei Li. Design and Application of an Optimum Backup Roll Contour Configured with CVC Work Roll in Hot Strip Mill. ISIJ International, 2012, 1637-1643. https://doi.org/10.2355/isijinternational.52.1637

Yan-Lin Li, Jian-Guo Cao. ASR Bending Force Mathematical Model for the Same Width Strip Rolling Campaigns in Hot Rolling. Steel Research International. 2014, 567-575. https://doi.org/10.1002/srin.201400133

Zhang Guo-min, Xiao Hong**.** Three-Dimensional Model for Strip Hot Rolling. Journal of Iron and Steel Research International, 2006, 23-26. https://doi.org/10.1016/S1006-706X(06)60020-4

ISSN-2531-2189

Article **Journal of Mechanical Engineering**
June, 2023 Vol.7 No.19 6-11

Fuzzy Modeling of DC Motors using the stimulus-response method

Modelado Difuso de Motores de CD usando el método de estímulo-respuesta

GONZÁLEZ-CASTOLO, Juan Carlos*†, RAMOS-CABRAL, Silvia, HERNÁNDEZ-RUEDA, Karen and ZATARAIN-DURÁN, Omar Alí

Universidad de Guadalajara

ID 1st Author: *Juan Carlos, González-Castolo* / **ORC ID**: 0000-0003-2659-0646, **Researcher ID Thomson**: R-5580-2018

ID 1st Co-author: *Silvia, Ramos-Cabral* / **ORC ID**: 0000-0003-4204-1700, **Researcher ID Thomson:** R-7124-2018

ID 2nd Co-author: *Karen, Hernández-Rueda* / **ORC ID**: 0000-0002-7209-2907, **Researcher ID Thomson**: AAM-4861-2021

ID 3nd Co-author: *Omar Alí, Zatarain-Durán* / **ORC ID**: 0000-0002-7934-7765, **Researcher ID Thomson**: E-2222-2019

DOI: 10.35429/JME.2023.19.7.6.11 Received: September 30, 2023; Accepted: December 30, 2023

Abstract

In this paper gives a brief review of the traditional modeling of *direct current* (DC) motors using the *stimulus response* method is made and a method is proposed to obtain an alternative model, using fuzzy logic theory. The two models capture the behavior of the DC motor in an acceptable manner. The connotation of acceptable is because some characteristics of the DC motor are disregarded, which do not have repercussions, in practical terms, as error factors in its study. The first model relates the analysis to the classical forms of control theory, through a first-order differential equation. The second model relates the analysis to the principles of generalization of necessary knowledge in reasoning and learning within the area of Artificial Intelligence where fuzzy sets and a series of if-then type rules are used. The fuzzy DC motor model is very convenient, within the control context, when using Artificial Intelligence paradigms but it not limited to this area.

Fuzzy Model, Control, DC motor

Resumen

En este artículo se hace una breve revisión del modelado tradicional de motores de *corriente directa* (CD) utilizando el método de estímulo respuesta y se propone un método para obtener un modelo alternativo, utilizando la teoría de lógica difusa. Los dos modelos capturan de forma *aceptable* el comportamiento del motor de CD. La connotación de *aceptable* obedece al hecho que, se desprecian algunas características del motor que no repercuten, en términos prácticos, como factores de error en su estudio. El primer modelo relaciona el análisis con las formas clásicas de la teoría de control, mediante una ecuación diferencial de primer orden. El segundo modelo, relaciona el análisis con los principios de generalización del conocimiento necesarios en el razonamiento y aprendizaje dentro del área de la Inteligencia Artificial, donde se utilizan conjuntos difusos y una serie de reglas del tipo si-entonces. El modelo difuso del motor es muy conveniente, dentro del contexto de control, cuando se utilizan paradigmas de Inteligencia Artificial pero no se limita a esta área.

Modelado difuso, Control, motor CD

Citation: GONZÁLEZ-CASTOLO, Juan Carlos, RAMOS-CABRAL, Silvia, HERNÁNDEZ-RUEDA, Karen and ZATARAIN-DURÁN, Omar Alí. Fuzzy Modeling of DC Motors using the stimulus-response method. Journal of Mechanical Engineering. 2023. 7-19: 6-11

* Correspondence to the Author (e-mail: jcgcastolo@gmail.com)
† Researcher contributing as first author.

Introduction

DC motors have wide popularity because they are very versatile in industrial (Kumar, Surya, Tabrez, Afida, & Molla Shahadat, 2022), domestic (Khan, *et al*., 2021), and laboratory (Said, *et al*., 2022) mechanical applications. In many industries, DC motors are used as elements that perform essential tasks within their processes. The wide uses of DC motors motivate many laboratory projects to address some control problems (Goolak, *et al*., 2023) without the need to disassemble the motor to bring it to the laboratory. In control projects of design and/or redesign of control loops, it is necessary to have mathematical models of the elements involved and, within context, of the DC motor (Cero, Vázquez-Espinoza, & Aquino-Díaz, 2017).

It is possible to obtain the motor structure representation of the motor behavior using the stimulus-response method (Nasimba Medina & Nasimba de Janon, 2018), that is, by analyzing motor response to a disturbance (Fang, *et a*l., 2023). Properly speaking about the transfer function. In general, the model with a first-order differential equation equivalence can be obtained (Haro Martínez, 1998).

In the existing bibliography, to analyze and design control loops in industrial processes or control projects, mathematical modeling of motors is performed based on time constants and motor torque (Valtchev, Meshcheryakov, Gracheva, Sinyukov, & Sinyukova, 2023). Practical implementation of a control system involves knowledge of these values, having as objectives, position, or speed control. An example of the usefulness of this work is in robotic systems (Zhao & Seung-Hoon, 2023), where there is a need to know the rotational position of joints in automotive assembly lines using representation models that are easily obtained without detriment to simple operation and/or understanding.

This paper is organized as follows: Section II overviews control and fuzzy logic theory. Section III presents the procedure to obtain the parameters of a first-order differential equation, represented in the complex plane, which models the DC motor. The process obtains the fuzzy rules modeling the motor is presented in Section IV. Finally, the conclusions are shown in Section V.

II. Background

A. Control theory

The analog control loop is represented by block diagrams which contain an algebraic mathematical expression (differential equations in the complex plane) (Dorf & Bishop, 2017). The equations contained in the blocks represent the behavior of the defined elements (plant, controller, transducer, etc.) as a function of the input-output. The relation between output and input is known as the *transfer function* (TF). The TF of the DC motor involves a couple of constants based on the physical characteristics of the motor. Knowing the value of these constants allows precise knowledge of the value of the angular position of the shaft, the applied speed-voltage relationship, and the motor torque.

B. Fuzzy logic theory

In possibility theory, a fuzzy set (FS) $\tilde{a}$ is used to delimit poorly known values and/or to represent values characterized by symbolic expressions (Kaufmann & Gupta, 1991). The set is defined as $\tilde{a} = (a_1, a_2, a_3, a_4)$ such that $a_1, a_2, a_3, a_4 \in \mathbb{R}$, $a_1 \leq a_2$ y $a_3 \leq a_4$ (Klir & Yuan, 1995) (Fig. 1).

Definition 1: A FS $\tilde{a}$ of a universe of discourse X={x} is defined as a mapping $\alpha_{\tilde{a}}: X \rightarrow [0, \gamma]$ where each $x \in X$ is assigned to a number in the range between $[0, \gamma]$.

FS $\tilde{a}$ is a membership $\alpha_{\tilde{a}}(x)$ of x elements, that are compatible with the $\tilde{a}$ concept.

Definition 2: FS is normal when membership function is normalized $\alpha_{\tilde{a}}: X \rightarrow [0,1]$.

A FS $\tilde{a}$ is referred to indistinctly by function $\alpha_{\tilde{a}}(\tau)$ or characterization (a_1, a_2, a_3, a_4), (Fig. 1).

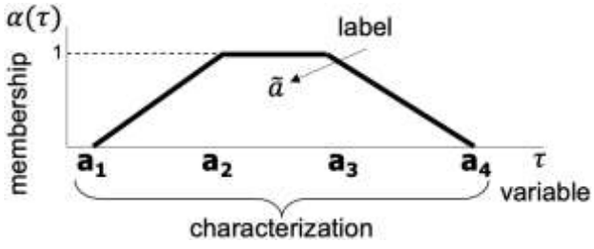

Figure 1 Fuzzy set representation
Source (González Castolo & López Mellado, 2009)

In this work, normal and trapezoidal FS will be used where $(a_2 = a_3)$, that is, triangular FS, $\tilde{a} = (a_1, a_2, a_4)$.

Definition 3: A *Fuzzy Rule* (FR) is identified as Rx with the form *if-then* where exists the antecedent and consequent represented by fuzzy sets;

Rx: if *antecedent* then *consequent*

III. DC motor model with the classical method

The physical system under study consists of a DC motor with a tachometer coupled to know when the motor reaches its maximum operating speed, (Fig. 2).

In most DC motors, the effect of the motor inductance L_a can be ignored because it is negligible with respect to the other values of the system. Under this consideration, simplifying the block diagram as Fig. 3(a), which indicates the ratio of the position $\theta(s)$ with respect to the supply voltage $E_{a_i}(s)$. Using this TF, the ratio of the speed and the supply voltage can be obtained, $W_o(s)/E_{a_i}(s)$. It is known that $w_o(t) = d(\theta)/dt$ in the complex plane remains as $W_o(s) = s\theta(s)$, (Fig. 3(b)).

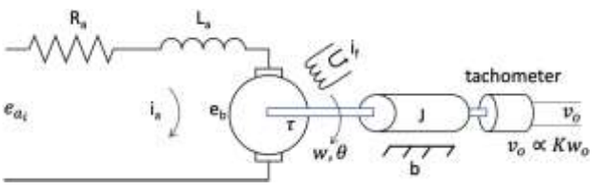

Figure 2 Motor physical system
Source: (Haro Martínez, 1998)

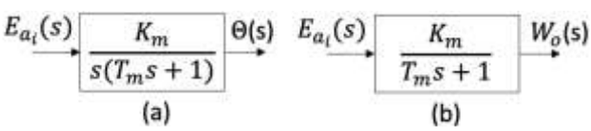

Figure 3 Motor transfer function
Source: (Haro Martínez, 1998)

The (1) is obtained by manipulating the *speed-supply voltage* relationship.

$$W_o(s)\left(\frac{K_m}{T_m}\right)\frac{1}{s+\frac{1}{T_m}}E_{a_i}(s) \tag{1}$$

The (2) is obtained considering that a unit step input is applied.

$$e_{a_i}(t) = \mu(t) \Longrightarrow E_{a_i}(s) = \frac{1}{s} \tag{2}$$

the values of K_m, (3), and T_m, (4), can be obtained.

$$K_m = c_1 \tag{3}$$

$$T_m = \frac{t_d}{\ln(2)} \tag{4}$$

With (3) and (4), the motor TF $W_o(s)/E_{a_i}(s)$ can be obtained.

This procedure boils down to measuring the motor response. The terminals of an oscilloscope are placed at the output of the tachometer and the nominal voltage applied $e_{a_i}(t)$ to the motor to obtain the graph of Fig. 4(a). The vertical axis has two variables with different scales because $v_o(t)$ is proportional to $w_o(t)$. The TF parameters of the motor (1) are calculate using (3) and (4). For example, the speed motor (7) with $t_d = 10$ time units and $c_1 = 1$ speed units the correspondent point is shows in Fig. 4(b) using (10).

$$w_o(t) = 1 - e^{-\frac{t}{14.4}} \tag{10}$$

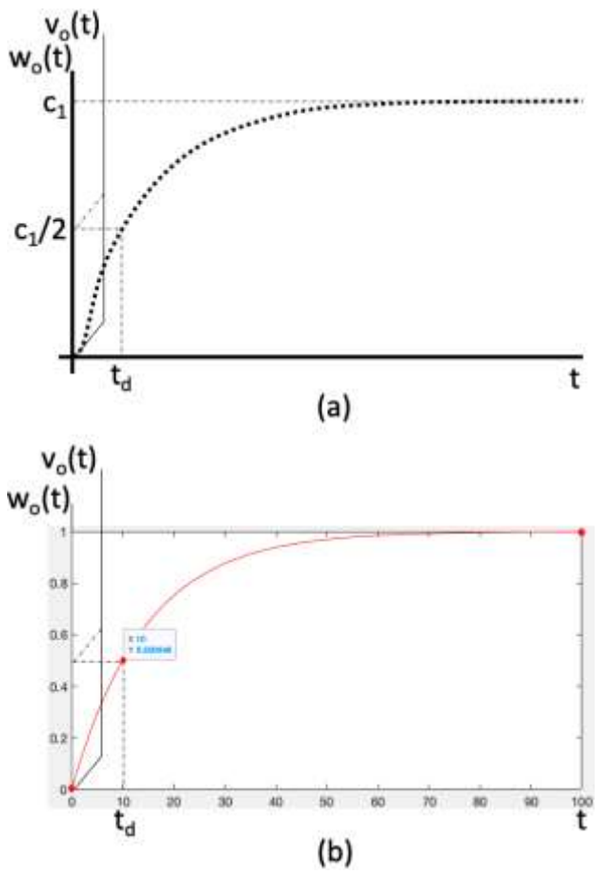

Figure 4 a) Voltage normalized of tachometer in oscilloscope. b) Mathematic $w(t)$ curve
Source: (Haro Martínez, 1998)

IV. Fuzzy logic DC motor model

A fuzzy version of the motor model is useful in control and automation applications using elements of Artificial Intelligence theory.

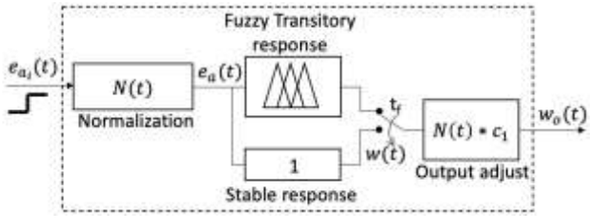

Figure 5 Fuzzy DC motor model
Own source

The fuzzy model has some blocks inside it, (Fig. 5). First, a *Normalization block* $N(t)$ guarantees that the variation of $e_a(t)$ will be in [0,1] range as is shown in (11).

$$N(t) = \frac{e_{a_i}(t)}{\max(e_{a_i}(t))} \tag{11}$$

The *Fuzzy transitory response block* (FTR(t)) is the output at time $[0, t_f]$, and this consists of fuzzy sets and fuzzy rules.

The *Stable response block* (SR) is the output after the input does not change, and this is time t_f.

Finally, the *Output adjust block* gives the speed $w_o(t)$ as shown in (12).

$$w_o(t) = (FTR(t) \vee SR)N(t)c_1 \tag{12}$$

For FTR(t), the Mamdani fuzzy inference method is used, which is more common and intuitive, in this case, than the Takagi-Sugeno method. For defuzzification, the centroid method is used.

Examining the motor response curves, (Fig. 4), the following work point are obtained: $(0,0)$, $(t_d, 0.5c_1)$, (t_f, c_1) where $t_d = 10$ and $t_f = 10t_d$. The t_f is the time when the output will be stable. In this example, $e_a(t) = e_{a_i}(t)$ because the input is the unit step.

To fuzzy model the behavior of DC motor, three fuzzy rules are proposed, (Table 1).

R1	**if** short-time **then** slow-speed
R2	**if** middle-time **then** average-speed
R3	**if** large-time **then** fast-speed

Table 1 Fuzzy Rules
Own Source

For the above rules, three FSs are proposed as antecedents and three FSs as consequents. The sets are defined in Table 2.

Antecedent (time)		Consequent (speed)	
short	$t_f(0,0,0.5)$	slow	(0,0,0.4)
middle	$t_f(0.03,1,1)$	average	(0,1,2)
large	$t_f(0.1,0.5,0.9)$	fast	(0.6,1,1.4)

Table 2 Fuzzy sets
Own Source

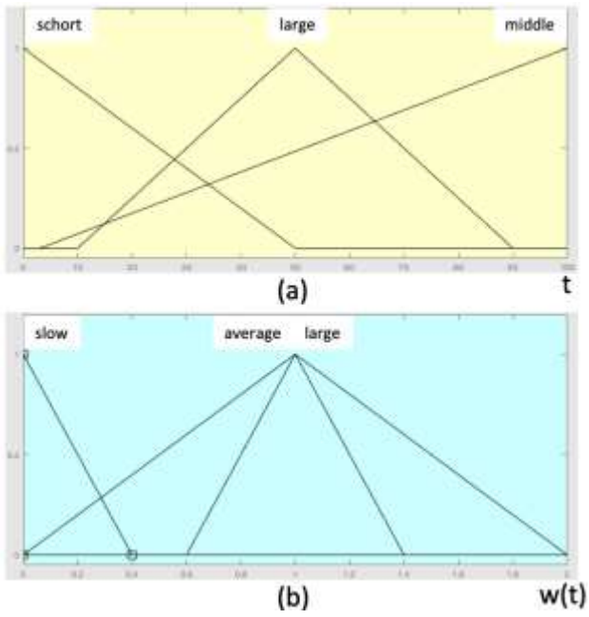

Figure 6 a) Antecedent fuzzy sets. b) Consequent fuzzy sets
Own Source

The range of variation of the antecedents and consequents can be from negative to greater than one. In this case, they are $(0, t_f)$, $(0,2)$, respectively. The sets used are shown graphically in Fig. 6.

Fig. 7 shows the fuzzy sets in the rules and the defuzzification (motor speed $w(t)$) for a specific time of *25* units. In this case, all antecedents in the rules have some degree of truth. Therefore, each has an answer that contributes to form the parallelogram whose centroid is the answer $w(25) = 0.845$. This calculus means that motor speed has *84.5%* of nominal speed c_1 at *25* time units.

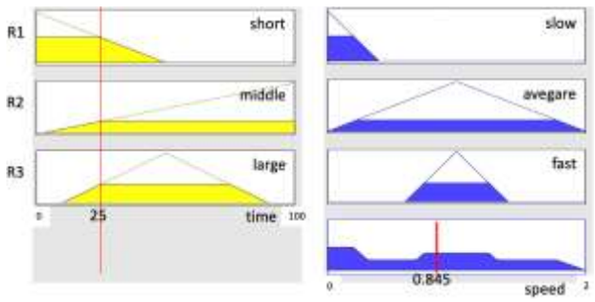

Figure 7 Defuzzification
Own Source

The motor response curve $w(t)$ is shown in Fig. 8. The point that corresponding to the calculation performed above for 25 time units is marked. After 100 time units, the response switches to *SR*.

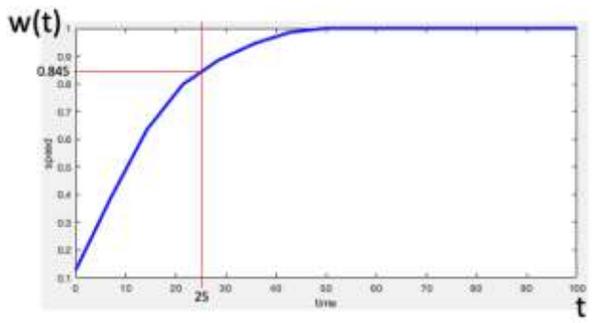

Figure 8 Motor response in time-speed relation
Own Source

Results comparison

The following table, Table 3, shows some results obtained (defuzzified values) and they are compared with the values of the motor response of the first model, (10). Here, $w_o(t) = w(t)$ because $c_1 = 1$.

Input (t) (time units)	Output of classical model $100(w_o(t))$	Output of fuzzy model $100(w(t))$
5	32	27.4
10	50	51
15	64	65.1
20	75	77.4
25	82	84.7
30	87	89.9
35	92	94

Table 3 Results comparison
Own Source

V. Conclusions

Some procedures for calculating the model of DC motors have been presented, and the results obtained are very reliable even though the base calculation process is approximate. It can be concluded that the fuzzy model is a good approximation of the motor behavior.

The importance of this procedure lies in the fact that it shows how a mechanical entity with intelligence features, based on experience, can improve the knowledge of its environment. If the robot controller is desired to be autonomous, adaptive, and causal, then an increasingly accurate reality can be reconstructed from the cause-effect relationship. In future work, a genetic algorithm will be used to find the improved fuzzy sets. In addition, based on the described procedure, thermal and hydraulic systems, among others, could be modeled with fuzzy sets using genetic algorithms to find these.

References

Cero, I., Vázquez-Espinoza, J., & Aquino-Díaz, E. (2017). Modelo matemático del motor de corriente directa. doi:10.13140/RG.2.2.27816.16645

Dorf, R., & Bishop, R. (2017). *Modern Control Systems 13th. Edition.* Pearson.

Fang, Q., Yong, Z., Shangjun, M., Chao, Z., Ye, W., & Haibin, H. (2023). Electromechanicl Actuator Servo Control Technology Based on Active DisturbancenRejection Control. *Electronics*, *12*(8). doi:https://doi.org/10.2290/electronics12081934

González Castolo, J., & López Mellado, E. (2009). *Fuzzy Approximation of DES State.* IGI Global. doi:10.4018/978-1-59904-849-9.ch102

Goolak, S., Liubarskyi, B., Riabov, I., Lukoševičius, V., Keršys, A., & Kilikevičius, S. (2023). Analysis of the Efficiency of Traction Drive Control Systems of Electric Locomotives with Asynchronous Traction Motors. *Energie*, *16*(9). doi: https://doi.org/10.3390/en16093689

ISSN-2531-2189

Haro Martínez, B. (1998). Congreso de Investigación UAG'98. *Procedimiento de laboratorio para el cálculo de las constantes de motores de CD*. Zapopan, Jalisco, México: UAG.

Kaufmann, A., & Gupta, M. (1991). *Introduction to Fuzzy Arithmetic, theory and applications.* Van Nostrand Reinhohld.

Khan, H. R., Majida, K., Haris, B. A., Muhammad Hashir, B. K., Abul, H., & Saad, A. Q. (2021). An Isolated Power Factor Corrected Cuk Converter with Integrated Magnetics for Brushless DC Ceiling Fan Applications. *Electronics, 10*(14). doi:https://doi.org/10.3390/electronics10141720

Klir, G., & Yuan, B. (1995). *Fuzzy Sets and Fuzzy Logic. Theory and Applications.* Prentice Hall.

Kumar, D., Surya, D. C., Tabrez, M., Afida, A., & Molla Shahadat, H. L. (2022). Model Antiseptic Control Scheme to Torque Ripple Mitigation for DC-DC Converter-Based BLDC Motor Drives. *Energies, 15*. doi:https://doi.org/10.3390/en15217823

Nasimba Medina, V., & Nasimba de Janon, J. (2018). Análisis de la eficiencia y características del par en función de la velocidad de un motor de corriente continua (c-d) con el campo en derivación. *Revista Publicando, 5*(18), 112-132.

Said, A., Félix-Herrán, L., Davizón, Y., Hernandez-Santos, C., Soto, R., & Ramírez-Mendoza, R. (2022). An Active Learning Didactic Proposal with Human-Computer Interaction in Engineering Education: A Direct Current Motor Case Study. *Electronics, 1*. doi:https://doi.org/10.3390/electronics11071059

Valtchev, S., Meshcheryakov, V., Gracheva, E., Sinyukov, A., & Sinyukova, T. (2023). Energy-Saving Control for Asynchronous Motor Motion System Based on Direct Torque Regulator. *Energies, 16*(9). doi:https://doi.org/10.3390/en16093870

Zhao, S., & Seung-Hoon, H. (2023). ROS-Based Autonomous Navigation Robot Platform with Stepping Motor. *Sensors, 23*(7). doi:https://doi.org/10.3390/s23073648

ISSN-2531-2189

Article **Journal of Mechanical Engineering**
June, 2023 Vol.7 No.19 12-22

Numerical and experimental analysis of the bodywork of a Formula SAE 2023 type vehicle

Análisis numérico y experimental de la carrocería de un vehículo tipo Formula SAE 2023

HERNANDEZ-URBANO, Cesar†, CORDERO-GURIDI, José de Jesús*, NOCHEBUENA-TIRADO, Carlos Jordán and VILLARREAL-CHAPA, José Ángel

Universidad Popular Autónoma del Estado de Puebla

ID 1st Author: *Cesar, Hernández-Urbano* / **ORC ID**: 0009-0002-2346-5364

ID 1st Co-author: *José de Jesús, Cordero-Guridi* / **ORC ID**: 0000-0001-5201-1906

ID 2nd Co-author: *Carlos Jordán, Nochebuena-Tirado* / **ORC ID**: 0009-0006-3789-6340

ID 3rd Co-author: *José Ángel, Villareal-Chapa* / **ORC ID**: 0009-0006-4227-3586

DOI: 10.35429/JME.2023.19.7.12.22 Received: March 30, 2023; Accepted: June 20, 2023

Abstract

In the present study, the aerodynamic characteristics of a bodywork for the Formula SAE 2023 competition were analyzed. Based on the requirements of the international competition regulations and the ISO 10521 standard, a numerical evaluation procedure was defined based on a CFD (Computational Fluid Dynamics) analysis. A bodywork model is presented and essential aerodynamic parameters were taken into account for the definition of the flow analysis models, where the k-omega model was used in the turbulent flow analysis. Additionally, an experimental analysis assembly was prepared through a wind tunnel at the University facilities, using a model of the bodywork by 3D printing at a scale of 1:43 with thermoplastic polyurethane material. Results of pressures, flow lines around the different elements of the bodywork were found, as well as drag coefficient values from 0.42 to 0.55, the latter were compared with others obtained by other Formula SAE teams, they found similarities in the results obtained. Additionally, with the wind tunnel, the comparison of the current lines was obtained, which showed similarities in the experiment and is expected to be improved in future studies.

Formula SAE, CFD, Aerodynamics, ANSYS

Resumen

En el presente estudio, se analizaron características aerodinámicas de una carrocería para la competencia Formula SAE 2023. En base a requerimientos del reglamento internacional de la competencia y la norma ISO 10521, se definió un procedimiento de evaluación numérica en base a análisis CFD (Computational Fluid Dynamics). Un modelo de carrocería es presentado y se definieron parámetros esenciales aerodinámicos a tomar en cuenta para la definición de los modelos de análisis de flujo, donde el modelo k-omega fue empleado en el análisis del flujo turbulento. Adicionalmente se preparó un montaje de análisis experimental mediante un túnel de viento en las instalaciones de la Universidad, empleando un modelo de la carrocería mediante impresión 3D a escala 1:43 con material de poliuretano termoplástico. Se obtuvieron resultados de presiones, líneas de flujo alrededor de los diferentes elementos de la carrocería, así como también valores del coeficiente de arrastre de 0.42 a 0.55, estos últimos se compararon con otros valores obtenidos por otros equipos de Formula SAE encontrado similitudes en los resultados obtenidos. Adicionalmente con el túnel de viento, se obtuvo la comparativa de las líneas de corriente, que mostraron similitudes en el experimento y se espera sean mejorados en estudios a futuro.

Fórmula SAE, CFD, Aerodinámica, ANSYS

Citation: HERNANDEZ-URBANO, Cesar, CORDERO-GURIDI, José de Jesús, NOCHEBUENA-TIRADO, Carlos Jordán and VILLARREAL-CHAPA, José Ángel. Numerical and experimental analysis of the bodywork of a Formula SAE 2023 type vehicle. Journal of Mechanical Engineering. 2023. 7-19: 12-22

* Correspondence to the Author (e-mail: josejesus.cordero@upaep.mx)
† Researcher contributing as first author.

Introduction

Formula SAE is an international competition, where university teams, made up of students, are put to the test for the design and manufacture of formula type competition cars; so they will have to put into practice all their skills, knowledge and technical skills in the development of the vehicle. The latter is put to the test in certain events that they will have to qualify for in order to gain points, thus winning the competition and recognition as the best design of that year.

Within the competition, there is a set of regulations which coordinates the requirements necessary for the teams to participate in the event, ensuring the functionality and safety of the vehicle for the different events. One of the elements of the regulations is related to the structure of the vehicle, which is an important element for both the integrity of the car and the necessary safety for the driver. Additionally, another point that is considered within the regulations is the bodywork, which is supported by the structure and has minimum guidelines for compliance with the regulations, but allows freedom of design.

As it is already known, aerodynamics has a great influence on the car, so this study must be done to improve the characteristics of the car; its safety, its comfort, its efficiency and its performance.

By studying the behaviour of the air flow in the car, we can obtain great results without adding a considerable amount of power to the car. One of the crucial factors in achieving high performance is an aerodynamic factor of the Formula SAE car itself. In addition, the most vital element in aerodynamics is downforce, lift, downforce and drag coefficient. Downforce is air load that pushes the top of the car to make more grip on the ground, to decrease wheel-to-floor slippage. Higher downforce means higher aerodynamic performance of the FSAE car [1].

CFD (Computational Fluid Dynamics) refers to the set of computational tools that, based on fundamental equations of fluid flow, allow predicting the behaviour of various engineering phenomena related to the behaviour and interaction of fluids and structures, as well as other similar phenomena.

Based on these tools, several studies have carried out CFD analyses for the validation of structures and vehicle bodies for the Formula SAE competition. Mariani F. et al [2] developed a numerical and experimental study to find the behaviour and critical numerical values for the performance of the bodywork for the Formula SAE competition, analysing the improvements with respect to previous versions of their vehicle.

On the other hand, Abid M. et al [3] developed experimental and numerical studies of the aerodynamic behaviour for their Formula SAE vehicle, describing the analysis properties for their wind tunnel and the relationship with CFD studies.

The relationship between the computational tools and the fundamental variables of aerodynamic analysis is critical to the improvement of the vehicle's dynamic properties, Deng Z. et al [4] describe their numerical studies, some of the equations that take part in the computational tools, while describing the variable pressures, velocities and distributions on the body of their vehicle.

Description of the Method

The development of this work was contemplated in 5 steps; which can be seen in the following diagram in Figure 1. The first step is the approach of the idea for the design of the bodywork, then and almost simultaneously followed the search for standards in which we will serve as a basis for making some of our decisions, then the experimental analysis was carried out to observe that the air around the body of the car really behaves in this way, then we will go to the use of software that will serve us for the modelling of the car and for the numerical analysis and, subsequently, we present results obtained from both analyses and the conclusions we reached about the idea proposed for the project.

ISSN-2531-2189

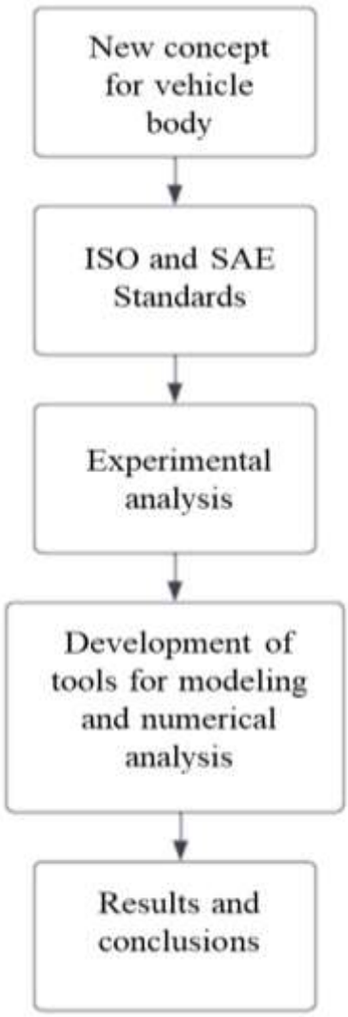

Figure 1 Method used for the research

Related to the standards that were applied; most of the bodywork is standardised especially for the FSAE 2023 competition, as another objective of this research is to test the proposed model and to test it in our favour. The standards used are found in section T.7, Body and Aerodynamic Devices. Additionally, concepts from ISO 10521[5] were used; which is external to the competition, but fundamental for the required analyses.

This standard suggests the test methods that should be used on a vehicle to know how it behaves with certain loads on level roads and with reference atmospheric conditions. Specifically, sections 6.1, 6.1.1, 6.1.2 and 6.1.3 were used, which is where you can find specifications for a wind tunnel, analysis of the same data, among other information that was very helpful.

In order to have more detail and control of the study, figure 2 shows a flow diagram, which was used by all the authors of this research, only for the numerical analysis in software.

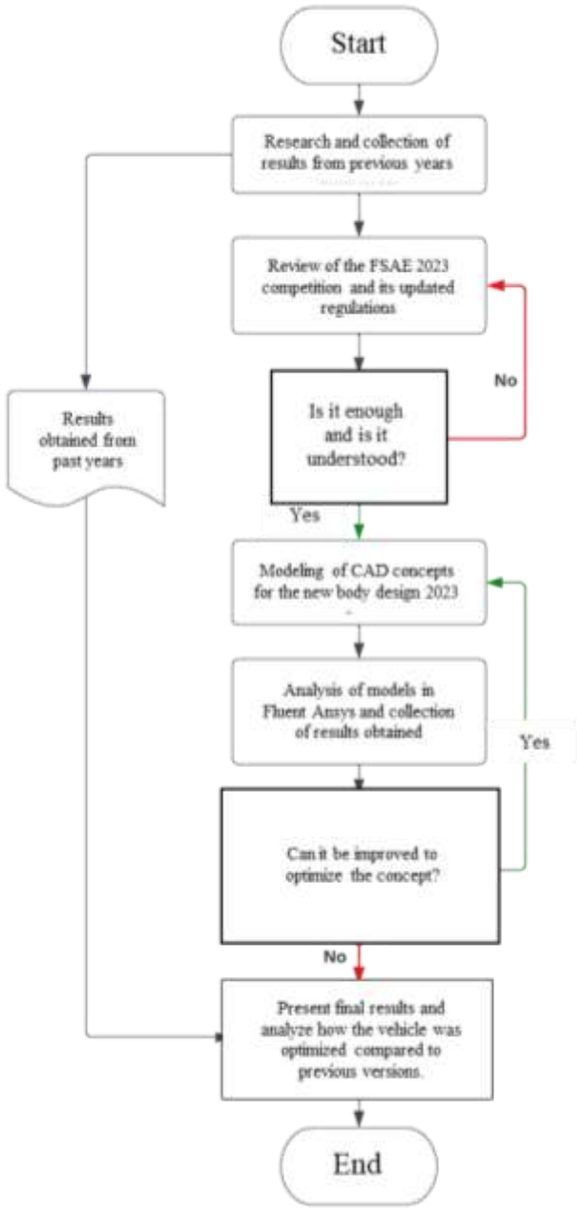

Figure 2 Method used for the numerical analysis

As can be seen in the previous graph (Figure 2), the experimental analysis is not included; this was because it was decided to do it partly because it was considered as a process by the numerical one.

Next, Figure 3 shows the flow chart to be used for the experimental method, once it has been analysed and used.

ISSN-2531-2189

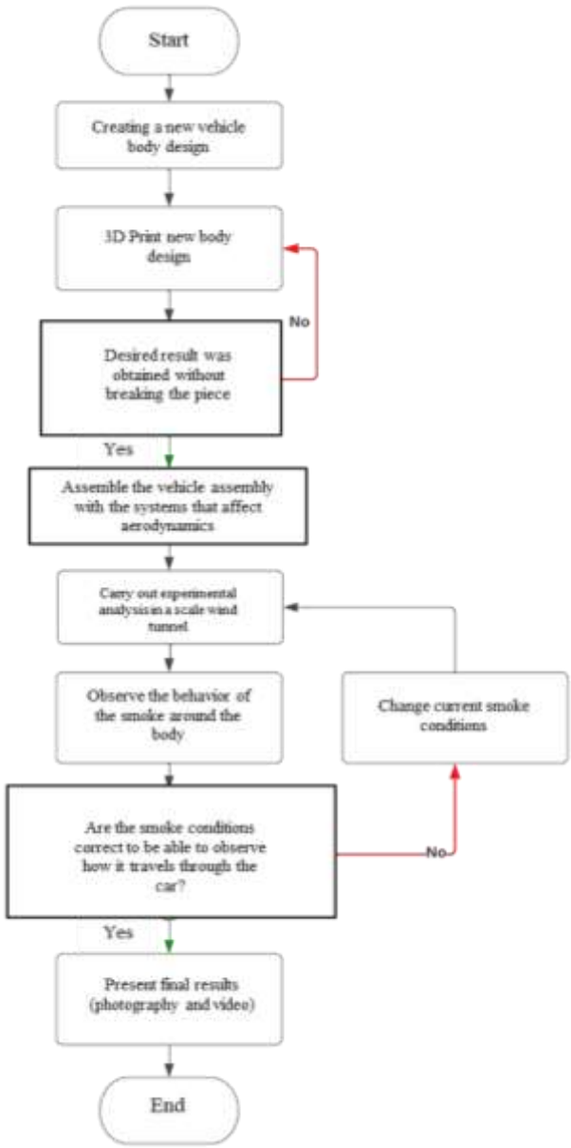

Figure 3 Experimental Analysis

Analytical Approach to the Problem

Within the numerical evaluations, and for a better mastery of the body development, several fundamental equations of fluid dynamics for Formula vehicles were investigated, which are presented below:

Bernoulli's principle

For aerodynamics, Bernoulli's principle is fundamental to understanding the flight of aeroplanes, helicopters, kites and other flying objects and generates the lift in the wings of an aircraft and how airflow is produced around its surface, an example for a Formula vehicle is shown in figure 4.

In fluid engineering it helps us to optimise the performance and efficiency of these systems and is expressed as shown in Ec. 1.

$$Cte = P + \frac{\rho V^2 gh}{2} \quad (1)$$

P is the pressure of the fluid at a given point.
ρ is the density of the fluid.
v is the velocity of the fluid at that point.
g is the acceleration due to gravity.
h is the height of the point relative to a reference level.

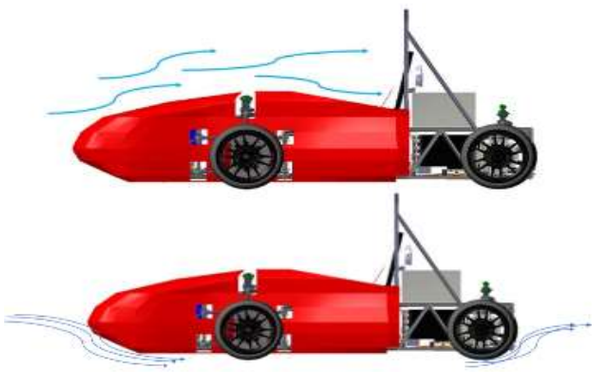

Figure 4 Pressures across the car

Drag force

This force acts in the opposite direction of motion and is proportional to velocity. Drag force is important in many applications, especially in aerodynamics and vehicle design. An example for a Formula vehicle is shown in figure 5.

The general formula for drag force is shown in Ec. 2.

$$F_D = \frac{\rho A V^2 C_D}{2} \quad (2)$$

F is the drag force.
ρ is the density of the fluid (e.g. density of air).
A is the reference area of the object perpendicular to the flow direction.
Cd is the drag coefficient, which depends on the shape and surface of the object.
v is the velocity of the object with respect to the fluid.

ISSN-2531-2189

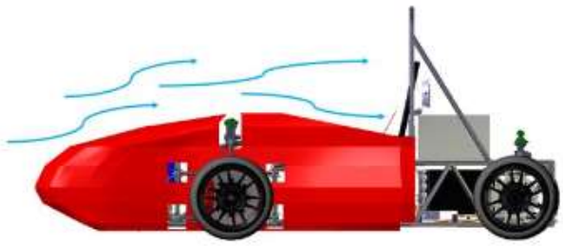

Figure 5 Drag force through the car

Drag Coefficient

It is worth mentioning that the lower the value, the better the aerodynamics of the car. An example for a Formula vehicle is shown in figure 6. The formula for calculating this coefficient is shown in Ec. 3.

$$C_D = \frac{F_D}{(A\frac{[\rho V^2]}{2})} \tag{3}$$

F is the drag force.
ρ is the density of the fluid (e.g. density of air).
A is the reference area of the object perpendicular to the flow direction.
Cd is the drag coefficient, which depends on the shape and surface of the object.
v is the velocity of the object with respect to the fluid.

Sustenance force

This effect has the effect of lifting the car while the car is in motion. An example for a Formula vehicle is shown in figure 6. The general lift force equation is shown in Ec. 4.

$$F_L = \frac{\rho V^2 A C_L}{2} \tag{4}$$

Cl is the lift coefficient.
F is the lift force generated by the object.
ρ is the density of the fluid surrounding the object.
v is the velocity of the object with respect to the fluid.
A is the frontal area of the object in the direction of motion.

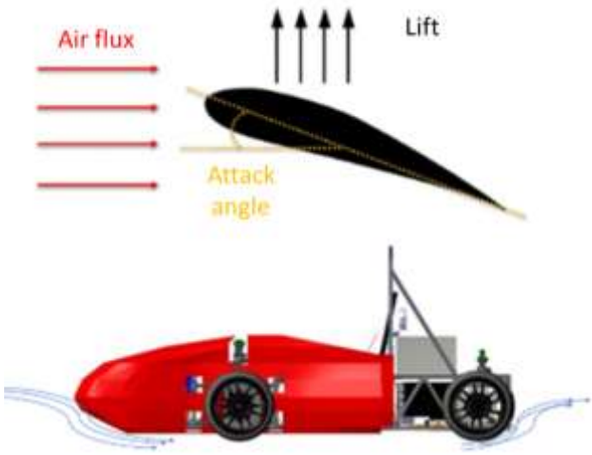

Figure 6 Representation of lift in an airfoil (Top) and lift through the car (Bottom)

Lift Coefficient

Defined as the ratio of the lift generated by the object to the dynamic pressure of the surrounding fluid. The lift coefficient is expressed mathematically as shown in Ec. 5.

$$C_L = \frac{2L}{\rho V^2 A} \tag{5}$$

Cl is the lift coefficient.
L is the lift generated by the object.
rho is the density of the fluid surrounding the object.
V is the relative velocity between the object and the fluid.
A is the frontal area of the object in the direction of motion.

The formula indicates that the lift coefficient is proportional to the lift generated by the object, the density of the fluid and the frontal area of the object, and is inversely proportional to the square of the relative velocity of the object and the fluid.

A higher lift coefficient indicates that the object can generate more lift for a given velocity and frontal area, which may allow it to lift or hover with less effort.

Reynolds number

Used to determine whether a flow is laminar or turbulent. It is calculated using the following formula shown in Ec 6.

ISSN-2531-2189

$$Re = \frac{\rho V L}{\mu} \quad (6)$$

Re is the Reynolds number.
ρ is the density of the fluid.
V is the velocity of the flow.
L is a characteristic length of the flow (e.g. the diameter of a pipe).
μ is the dynamic viscosity of the fluid.

If the value of Re is greater than the threshold, the flow is turbulent and the particles move in a chaotic and irregular manner.

Turbulent Flow

Turbulence is also characterised by recirculation, eddies and apparent randomness. In turbulent flow, the velocity of the fluid at a point is undergoing continuous changes in both magnitude and direction, as seen in figure 7.

Turbulent flow can occur when the Reynolds number (Re) exceeds a certain threshold. The Reynolds number is a dimensionless measure that relates the velocity of the fluid, its density, viscosity and a characteristic length of the flow. When the value of Re is high, inertial forces dominate over viscous forces, leading to turbulence.

The main tool available for their analysis is CFD analysis. It is widely accepted that the Navier-Stokes equations (or the simplified Reynolds-averaged Navier-Stokes equations) are capable of exhibiting turbulent solutions, and these equations are the basis of essentially all CFD codes. For this study the Reynolds number was evaluated in order to understand whether it was turbulent or laminar flow, a value of 3.70 x 10^2 was obtained which is well over 4000, if it was less than this it would be laminar flow; therefore, the model used for the resolution of the analysis was the k-omega.

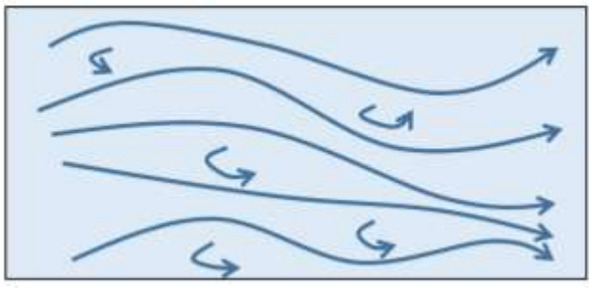

Figure 7 Turbulent flow

Technical Characterisation

Currently our car already has a bodywork which was taken to the Formula SAE 2022 competition, and we have as a basis the following characteristics that we consider important to take for the next proposal of the new bodywork 2023. The data are:

– Length: 1900 mm
– Width: 900 mm
– Height: 600 mm
– Thickness: 3 mm
– Fixings: 7
– Weight: 1,177 kg
– Area: 19.618 m2

Proposal

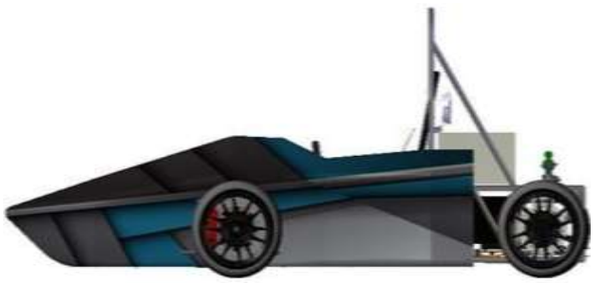

Figure 8 Proposal to be analysed

For our proposal we took into consideration all aerodynamic points -- possible, but at the same time applying all the rules provided by Formula SAE. At the time of designing the proposal we were taking different strategies with the use of CATIA V5 software in order to represent the idea of the sketch in 3D. In the proposal we considered in the smallest detail the way the wind attacks the vehicle in order to design it as aerodynamic as possible where the body itself helps to redirect the air in its favour, thus ensuring that proposal three is the one that had the best behaviour.

Numerical Analysis

Analysis Model

Having chosen proposal 3 we proceeded to make a fully solid geometric model in Catia V5 software, the model had slight geometry imperfections and these were corrected with the help of the SpaceClaim tools in Ansys.

ISSN-2531-2189

In the same Ansys space, an enclosure is created which helps to extract the existing solids in SpaceClaim and thus work in the analysis with Watertight Geometry, thus reducing the computational load and time in the analysis. On the other hand, a volume is generated to delimit where the analysis is performed and to be able to determine the interaction of the air with the model, thus simulating its functionality in a wind tunnel in the best possible way.

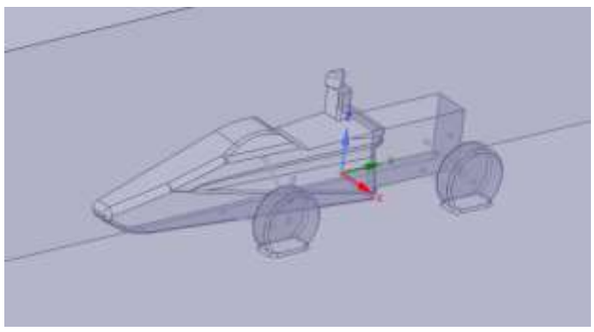

Figure 9 Extracted Solid (Watertight Geometry)

Bodies of Influence are also generated in order to control and refine the regions of interest during the meshing phase.

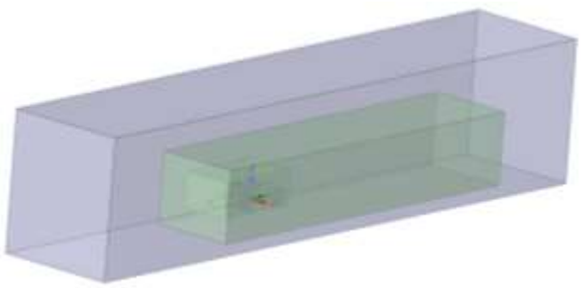

Figure 10 Wind tunnel and bodies of influence

Meshing

For the meshing phase, the corresponding local meshes had to be added for the Bodies of Influence as well as for the different regions with curvatures. It is also important to capture the effect on the boundary layers, so that the physics of the fluid flow in the thinner regions can be obtained accurately. By taking these parameters into account, a sufficiently reliable mesh volume is generated to perform the analysis correctly. A parameter to consider a reliable mesh is if its orthogonal quality remains below 0.1. A value of 0.089 was obtained, so we proceed without any problem to the resolution of the analysis.

Figure 11 Meshing through the Body

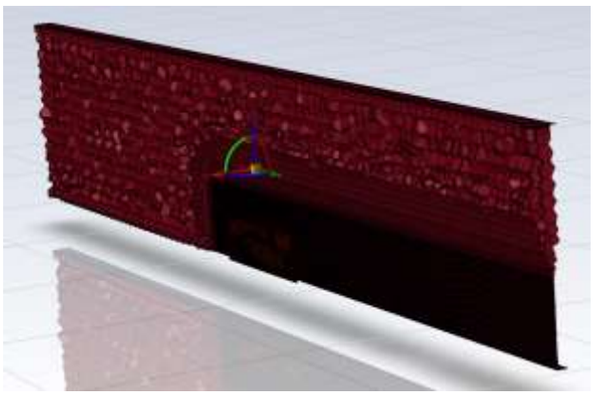

Figure 12 Wind tunnel meshing

Boundary conditions

For the resolution of the analysis it is necessary to make some adjustments to the computational domain previously verified, for this type of analysis, the model must be kept completely stationary, that is to say, all solids must be considered as non-slip walls, the walls that compose the enclosure will be considered as slip walls. For the slip walls, the inlet channel called Inlet and the floor must be set to a velocity of 20 m/s. In this way, a faithful representation of the functioning of a moving wind tunnel was achieved. With the dimensions of the solid model and the viscous properties of the air, its Reynolds number was calculated, which was 3.70 x10^6, thus confirming that the type of fluid flow involved is turbulent.

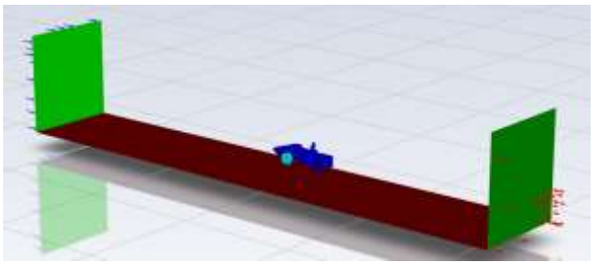

Figure 13 Wind tunnel view in software solver

ISSN-2531-2189

Condition	Reference values
Fluid velocity	20 m/s
Pressure	101325 Pa
Density	1.29 kg/m3
Fluid Type	Turbulent
Frontal Area	0.3133 m^2

Table 1 Boundary conditions of analysis

Experimental Analysis

In the development of the experimental analysis, a wind tunnel located in the engineering laboratories of the university was used. Initially, the analysis model of the vehicle was developed, for which a 1:43 scale model of thermoplastic polyurethane was manufactured in 3D printing, which is based on the similarity with the numerical model presented previously. The model is shown in figure 14.

Figure 14 3D printing of the FSAE model

Once the model was available, the aerodynamic analysis was carried out inside the institution's laboratories using an acrylic wind tunnel, as shown in figure 15.

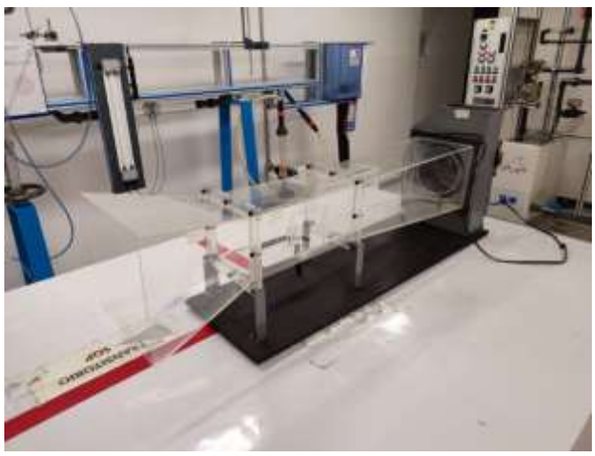

Figure 15 Wind tunnel of the university's engineering laboratories

This set-up allowed us to physically observe the graphical representation of what had already been analysed with the programmes with the help of a smoke machine. The car model was placed in the middle part of the tunnel and by means of a smoke machine and with the help of an air extractor at the back of the tunnel we were able to simulate the behaviour of the air through the car.

The wind tunnel has a length of 30 cm for the analysed area with a width of 15 cm and a height of 15 cm. The air extractor and the 1250w wired controlled smoke machine were used to obtain the results mentioned above.

Results

Once the analysis was finished, we obtained the results that will help us to understand the behaviour of the model. We obtained the forces and the general drag coefficient which was 0.66, also the forces and the general lift coefficient which was 0.8321. In addition, as shown in the static pressure Contour Plot in figure 16, the behaviour of the air over the model can be observed, the pressure difference ranges from -250 Pa to 262 Pa. Taking Bernoulli's principle as a reference, it is possible to perceive the highest pressure points that are located both in the wheels and in the nose of the body, these results were to be expected due to its positioning being the first point of contact with the air, however, knowing this data will benefit us for future implementations in order to improve the performance of the car.

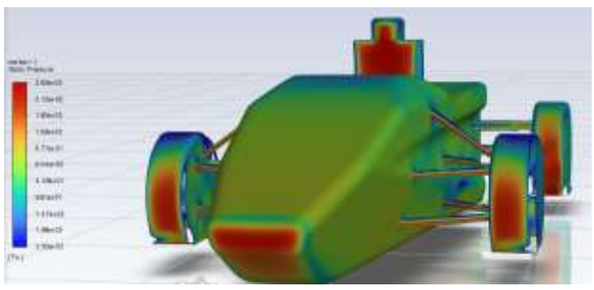

Figure 16 Static pressure contour plot of the analysed model

Another expected result to understand the currents generated around the car were the streamlines as shown in pictures 17 to 19. In this way we can find deficiencies, leaks or simply turbulence generation, and it is also part of the experimental representation in the wind tunnel of the University.

ISSN-2531-2189

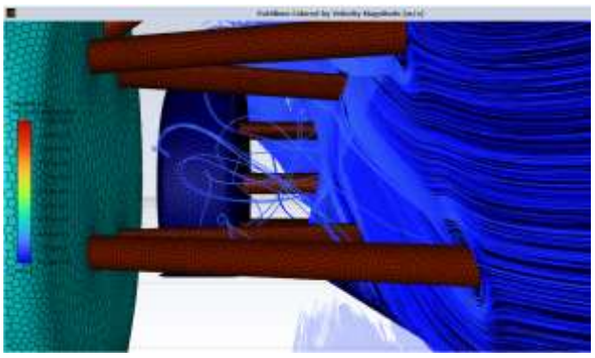

Figure 17 Power lines through suspension arms

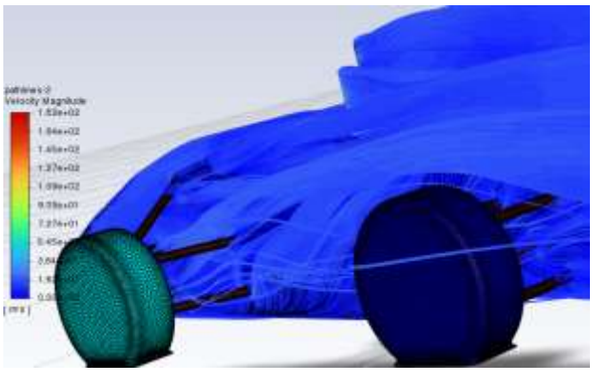

Figure 18 Power lines through the model (Rear view)

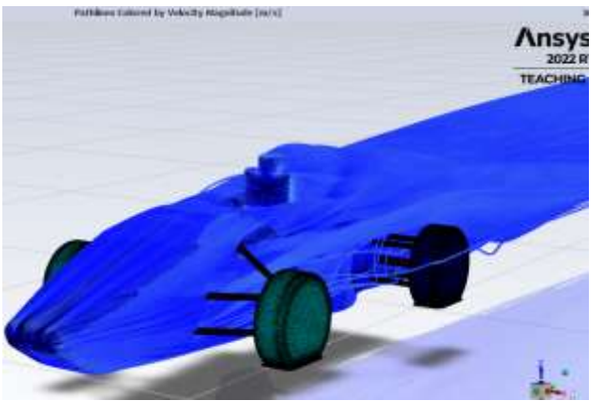

Figure 19 Streamlines through the model (Isometric view)

As shown in figure 20, with the help of vectors we can notice the meshing differences with respect to each Body of influence, and also the recirculation regions.

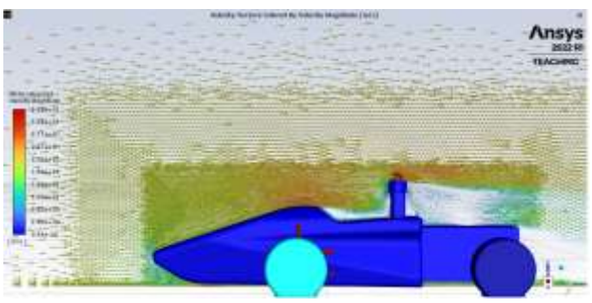

Figure 20 Streamlines in the wind tunnel

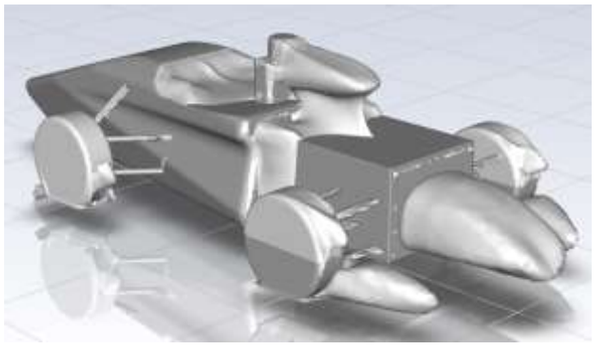

Figure 21 Recirculation regions in the model

Regarding the experimental analysis, the following images were obtained from the wind tunnel analysis, in perspective as shown in figure 22 and lateral as shown in figure 23.

Figure 22 Prototype vehicle current flow lines

Figure 23 Current flow lines on prototype vehicle in side view

In the image above we can see how the vehicle is surrounded by the smoke we launched, with streamlines similar to those shown in the numerical studies, although with some differences in the section of the pilot and the interaction with the stream.

ISSN-2531-2189

Conclusion and discussion

In the results shown, studies were obtained to determine highly relevant data for vehicle design, such as drag coefficient values with and without aerodynamic devices (wings, spoiler, splitter, sideskirts, diffuser) within which average values of 0.55 with devices and 0.42 without aerodynamic devices were obtained.

Several studies were taken to analyse the results obtained for the drag coefficient, where Mariani F. et al [2] found a value of 0.46 in their experimental study. Regarding other studies, Mohanan A. et al [6] found in the study of bodywork and other aerodynamic accessories a value of 0.584. Abid M. et al [3] in their numerical and experimental approach found a value of 0.57. Additionally, Οξύζογλου, I. N. [7] found in his thesis a value of 0.426. This is shown in graph 1.

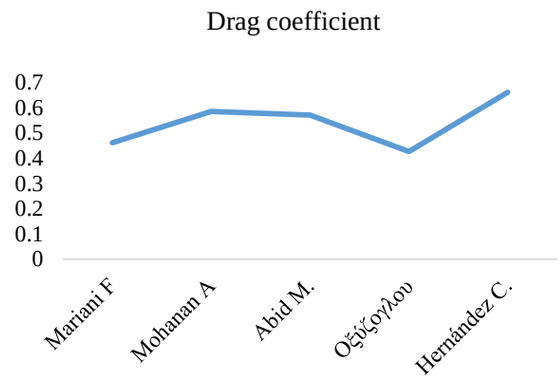

Graph 1 Comparison of drag coefficient results for Formula SAE vehicles

Based on the results obtained and the comparison of figure 24, as well as the observation of the flow lines in the experimental wind tunnel, we can conclude that the flow paths of the prototype and the drag coefficient generated was ideal, as it is in the expected range compared to research from other universities. It should be stressed that the implementation of aerodynamic components influences the performance of the car, more aerodynamic components means a higher drag coefficient, but if done correctly it implies a negative lift generation which undoubtedly improves the performance of the car. Therefore, the analysed body has a wide base of information to understand the aerodynamic behaviour around the FSAE vehicle of the university, for future research it is advisable to use this body as a base to add aerodynamic components and thus gradually improve the performance of the car.

It is important to mention that in the development of the experimental analysis there were some problems, as there were not enough resources to put all the measurements that were defined in the computational analysis, this implies that, in later works, the necessary instrumentation will be installed to measure different characteristics. Also, with the aim of improving the results, some variables can be improved, a very clear example is the smoke; treating it so that it has a denser appearance is important, as in the first attempts in this study it was not possible to see it properly, so it was decided to modify its colour and density. The application of the experimental current is also important, since it facilitates the visualisation of the results. In this procedure, after making changes in these variables, better results were obtained and it was much better visualised how the currents around the trolley behave.

Acknowledgements

The authors would like to thank the Universidad Popular Autónoma del Estado de Puebla, for the use of the facilities and the facilities granted in the development of this work.

Funding

This work was fully supported by the Universidad Autónoma del Estado de Puebla A.C.

References

[1] Dharmawan, M. A., Ubaidillah, U., Nugraha, A. A., Wijayanta, A. T., & Naufal, B. A. (2018b). Aerodynamic analysis of formula student car. Nucleation and Atmospheric Aerosols. https://doi.org/10.1063/1.5024107

[2] Mariani, F., Poggiani, C., Risi, F., & Scappaticci, L. (2015). Formula-SAE racing car: Experimental and numerical analysis of the external aerodynamics. Energy Procedia, 81, 1013-1029.https://doi.org/10.1016/j.egypro.2015.12.111

[3] Abid, M., Wajid, H. A., Iqbal, M. Z., Najam, S., Arshad, A., & Ahmad, A. (2017). Design and analysis of an aerodynamic downforce package for a Formula Student Race Car. IIUM Engineering Journal, 18(2), 212-224.https://doi.org/10.31436/iiumej.v18i2.679

ISSN-2531-2189

[4] Deng, Z., Yu, S., & Wu, C. (2020, July). Numerical Simulation and Analysis for Aerodynamic Devices of FSAE Racing Car. In Journal of Physics: Conference Series (Vol. 1600, No. 1, p. 012079). IOP Publishing. https://doi.org/10.1088/1742-6596/1600/1/012079

[5] ISO, B. (2006). 10521-2: 2006 Road vehicles. Road load. Part, 1.

[6] Mohanan, A., Pandey, J. A., Gupta, A. V., Almeida, S. G., & Choudhari, D. Development of External Aerodynamics of an FSAE Racecar using Computational Fluid Dynamics. https://doi.org/10.4271/2015-36-0359

[7] Οξύζογλου, Ι. Ν. (2017). Design & developement of an aerodynamic package for a FSAE race car (Bachelor's thesis). https://ir.lib.uth.gr/xmlui/handle/11615/49094

ISSN-2531-2189

Article **Journal of Mechanical Engineering**
June, 2023 Vol.7 No.19 23-31

Comparison of microstructure and mechanical properties of industrial pure aluminum produced by powder metallurgy and conventional rolling

Comparación de microestructura y propiedades mecánicas de aluminio industrialmente puro fabricado por laminado convencional y metalurgia de polvos

SALGADO-LÓPEZ, Juan Manuel†*, MARTINEZ-FRANCO, Enrique, CRUZ-GONZÁLEZ, Celso Eduardo and TELLO-RICO, Mauricio

Centro de Ingeniería y Desarrollo Industrial CIDESI

ID 1st Author: *Juan Manuel, Salgado-Lopez* / **ORC ID**: 0000-0002-2384-1887, **CVU CONAHCYT ID**: 94744

ID 1st Co-author: *Enrique, Martinez-Franco* / **ORC ID**: 0000-0001-8412-7778, **CVU CONAHCYT ID**: 81630

ID 2nd Co-author: *Celso, Cruz-Gonzalez* / **ORC ID**: 0000-0001-7620-9052, **CVU CONAHCYT ID**: 357789

ID 3er Co-author: *Jesús Mauricio, Tello-Rico* / **ORC ID**: 0000-0002-5657-2134, **CVU CONAHCYT ID**: 586320

DOI: 10.35429/JME.2023.19.7.23.31 Received: March 30, 2023; Accepted: June 30, 2023

Abstract

Aluminum alloys are produced by different manufacturing techniques and each technique produces a unique microstructure. One of the most versatile manufacturing methods is powder metallurgy (P/M) because it produces a final fine or ultrafine grain microstructure. But it requires powder consolidation and densification processes after P/M. In the other side, Hot Isostatic Pressing (HIP) is now recognized as a very interesting technique to densify advanced materials with a high potential. The aims of this work are: to produce an AA1100 aluminum billet by powder densification followed by HIP and to compare its microstructure and mechanical properties against the ones of an AA1100 aluminum plate produced by conventional rolling. The mechanical properties were measured using tensile test and Charpy test. The results show that the tensile strength of the P/M+HIP sample is higher than the one of the aluminum plate, but the yield strengths are similar. In the other hand the impact toughness results are very different from each other.

Alloy, Microstructure, Property

Resumen

Las aleaciones de aluminio se producen mediante diferentes técnicas de fabricación y cada técnica produce una microestructura única. Uno de los métodos de fabricación más versátiles es la metalurgia de polvos (P/M) porque produce una microestructura final de grano fino o ultrafino. Sin embargo, este método requiere de procesos de consolidación y densificación de polvo posteriores. El prensado isostático en caliente (HIP) es una técnica ampliamente utilizada para densificar materiales obtenidos por P/M, fundiciones comerciales y los nuevos materiales producidos por manufactura aditiva. Los objetivos de este trabajo son producir un tocho de aluminio AA1100 por densificación de polvo seguido del proceso HIP para comparar su microestructura y las propiedades mecánicas contra las de una placa de aluminio producida por método convencional. Las propiedades mecánicas fueron medidas mediante ensayo de tracción y ensayo Charpy. Los resultados muestran que la resistencia a la tracción de las muestras de P/M+HIP es mayor que las muestras de la placa de aluminio, pero los límites elásticos son similares. Por otro lado, los resultados de la tenacidad al impacto difieren fuertemente entre ambos materiales.

Aleación, Microestructura, Propiedades

Citation: SALGADO-LÓPEZ, Juan Manuel, MARTINEZ-FRANCO, Enrique, CRUZ-GONZÁLEZ, Celso Eduardo and TELLO-RICO, Mauricio. Comparison of microstructure and mechanical properties of industrial pure aluminum produced by powder metallurgy and conventional rolling. Journal of Mechanical Engineering. 2023. 7-19: 23-31

***** Correspondence to the Author (e-mail: msalgado@cidesi.edu.mx)
† Researcher contributing as first author.

Introduction

Aluminum alloys are in great demand in various industrial sectors, as they offer a good agreement between strength and density, as well as being relatively cheap [1]. Aluminum alloys are large family of alloys with a variety of alloying elements, but not all Al alloys behave similarly when they are processed by the different manufacturing methods due to the difference in alloy elements and compositions [1-3]. There are many processing routes to produce aluminum alloys and each of them leads to a unique microstructure and mechanical properties. Among all the manufacturing techniques one of the most versatile is powder metallurgy (P/M), because it allows to alloy beyond the equilibrium concentration different metals and no metals, while at the same time it produces a final microstructure with fine or ultrafine grain structures. It P/M has been successfully applied for alloying aluminum with elements such as: Si, Al, Cu, Mg, etc. but also to fabricate nanocomposites of aluminum with different reinforcement particles such as yttrium oxides, aluminum oxides, carbon nanotubes, etc. [4-12].

The high energy grinding process produces the formation of agglomerates and by controlling the processing parameters it is possible to reduce the amount and size of said agglomerates, which translates into an increase in the production efficiency of processed powders. The processing of powders through cycles at high and low revolutions favors control in agglomerates as a result of the interactions between balls and particles [13-17].

Powder metallurgy requires powder consolidation and densification processes after the powder particles are processed in a high-energy ball mill. Some of the densification techniques applied for getting useful products are: strained powder rolling, sinter forging, or Hot Isostatic Pressing (HIP). Among those processes, HIP is now recognized as a very interesting technique to densify advanced materials with a high potential and it is the way to optimize material properties [7- 10].

HIP is defined in ASTM B998-17 as a process were components are subjected to the simultaneous application of heat and high pressure in an inert gas medium [11].

The process is used for the reduction of internal (non-surface connected) porosity. It is considered as efficient method for improving mechanical properties for a great variety of alloys and it is recommended also for additive manufacturing components. In this way, HIP is becoming the standard method to improve lifetime of critical parts. Common applications for HIP in the industry are: closed porosity removal, consolidation of powders and diffusion bonding of dissimilar metals or alloys [7-13].

In literature there is much information about composites, nanocomposites and aluminum alloys powders consolidated using HIP [4-12]. However, there is too few information about consolidated pure aluminum powders using this method and its final mechanical properties. Therefore, the aims of this work are: to produce an AA1100 aluminum billet by powder consolidation in Hot Isostatic Pressing (HIP) and to compare the microstructure and mechanical properties measured using tensile test and Charpy test against the ones of aluminum AA1100 plate produced by conventional rolling.

Methodology

In this work, the aluminum powders were processed in a high-energy ball milling (HEBM) commercially named as Simoloyer CM01 with capacity of 2000 ml in volume (figure 1). The grinding parameters used were 850rpm/5min and 250rpm/1min until reaching 50 minutes of processing. In this case, only the time at high speed was considered as process time. Figure 1 shows the HEBM system with the adaptations for the control of the atmosphere prior to start of the process, as well as the control program.

The processed powders were passivated in a specially designed and manufactured for this purpose container with a controlled amount of oxygen. The operation was carried out in vacuum within the container that was located on rotating rollers. Then air was slowly introduced in several stages. Since the passivation process is exothermic, the temperature in the system need to be monitored. This process was finished when no change in the temperature was registered. The rotation by means of the rollers allowed the homogeneous passivation of the powders.

ISSN-2531-2189

Powders processed by HEBM have different morphology as raw materials and particle size distribution is normally broad. Therefore it is necessary operations as sieving in order to get the suitable distribution particles sizes for sintering using HIP. For the sintering of aluminum powders, particles larger than 250 microns in size were separated, because they make consolidation difficult due to the increase in spaces among particles, which leads to greater interaction distances among them and generating porosity in the solid component.

Figure 1 HEBM e equipment for powders processing

Powder encapsulation required a series of sequential operations that determine the success of powder consolidation by means of HIP process. The procedure activities are depicted in figure 2 and 4:

Figure 2 Welding of the powders containers for sealing the container

Figure 3 PT to verify the integrity of the container´s welding

After verifying that the encapsulation did not have porosity throughout the weld and it maintained a vacuum, consolidation was carried out by HIP.

Dye Penetrant testing (PT) and vacuum testing were carried out for assessing if the powder encapsulation was sealed.

The consolidation of the powders by HIP had as process parameters: temperature, time and isostatic pressure of the argon gas used. In this work a Quintus Hot Isostatic pressing equipment was employed for consolidation system and the parameters were: 550 °C, 125 MPa and 5 hours. The results obtained from the HIP treatment of the encapsulated powders with the selected treatment parameters are shown in Figure 4.

Figure 4 Billet produced by HIP densification and transversal cut.

The visual inspection of the container indicated deformation, which meant a successful sintering of powders.

ISSN-2531-2189

The integrity of the weld throughout the package was also assessed by visual testing. The upper and lower covers of the encapsulation were removed by mechanical cuts. From this point, this billet is denominated as P/M+HIP Billet. The P/M+HIP billet obtained was nondestructive inspected using an X-ray microfocus CT cabinet system for 3D metrology and analysis model PHOENIX V/GTOME/XM.

For comparison an AA11010 aluminum plate was used. The chemical composition was determined by the same techniques applied in the P/M+HIP billet. The chemical composition of the aluminum plate, and the powder encapsulation was determined by Optical emission spectrometry using an OBLF Optical emission Spectrometer QSN-750-II.

The mechanical properties were measured using a universal testing machine SHIMADZU WADE AGX-V 100KN following ASTM E8/E8M-21. For this tests a class B extensometer was used. The Charpy test was carried out using a SATEC model CHARPY impact pendulum according to ASTM E23/E23-18. Samples for tensile and Charpy impact testing were taken at 0°, 45 ° and 90° from the rolling direction of the AA110 aluminum plate; but due to the dimensions of the aluminum P/M +HIP billet only sub size samples were taken.

Samples were cut from the aluminum plate and the P/M+HIP billet for metallographic preparation following ASTM E37E3M -17. After that they were mounted in conductive Bakelite and grinded from 120 to 2000 SiC grinding paper. The samples were polished using 1 μm alumina powder slurry and a final polishing was carried out using diamond paste as polisher. A final etching step was performed using Keller´s as a reagent for revealing the microstructure. The observation was made with a NIKON EPIPHOT 200 optical microscope was carried out using a Nikon Optical microscope with ZEISS image analysis. Fractographic analysis of the Charpy and tensile tested samples was carried out using JEOL JSM 6610LV scanning electron microscope (SEM).

Results

The chemical composition of the aluminum AA1100 plate produced by conventional rolling and the P/M+HIP billet were determined. The results are shown in table 1, there is seen that the content of alloying elements shows small differences but the aluminum weight percentage was the same in both cases.

	% Cu	% Fe	% Mn	% Si	%Zn	% Ti	% Al
AA1010 standard	0.05-0.20	0.05 max.	0.05 max	NA	NA	NA	99.80 - 99.655
Al billet	0.00	0.01	0.00	0.11	0.02	0.01	99.71
AA1100 plate	0.00%	0.16	0.01	0.07	0.01	0.01	99.71

Table 1 Chemical composition of the aluminum AA1100 plate produced by conventional rolling and a billet produced by HIP

The P/M+HIP billet was nondestructive inspected by an X-ray microfocus CT cabinet system and the results showed evidence of aligned porosity of both types: connected and no connected (figures 5 to 7). Moreover, neither cracks nor laminations were detected. The results are shown in figures 6 and 7.

The microstructure of the P/M+HIP billet is seen in figure 8. There are seen fine grain size equiaxied grains and no evidence of precipitates nor second phases. There is seen good densification of the powders. Besides no evidence of connected porosity was found in the microstructure.

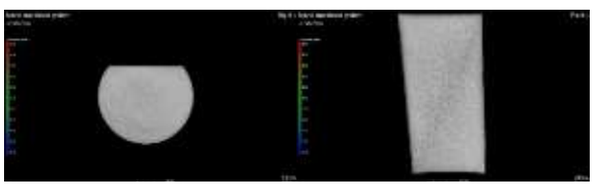

Figure 5 Images of the billet produced by HIP using X-ray microfocus CT cabinet system for 3D metrology and analysis model PHOENIX V/GTOME/XM

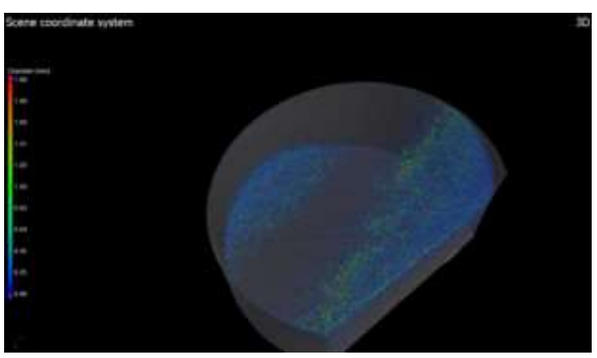

Figure 6 Image of the billet produced by HIP using X-ray microfocus CT cabinet system for 3D metrology and analysis model PHOENIX V/GTOME/XM

ISSN-2531-2189

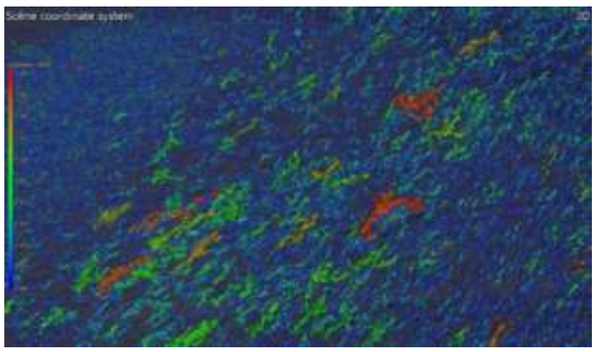

Figure 7 Image of the billet produced by HIP using X-ray microfocus CT cabinet system for 3D metrology and analysis model PHOENIX V/GTOME/XM.

Figure 9 shows the microstructure of the AA1100 aluminum plate produced by conventional method. There are seen equiaxial grains and no second phases. This microstructure matches with the reported information in literature. Room temperature tensile tests were conducted to determine mechanical properties following ASTM E8/E8M-21. Moreover, the impact toughness was measured by using the standard for the Charpy V-notched bar impact tests following E23/E23-18. The results of tensile test are shown in graphic 1 and table 2.

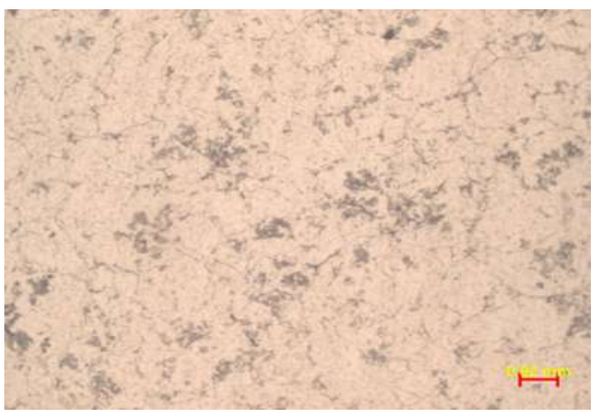

Figure 8 Microstructure at 500x of the billet produced by P/M+HIP

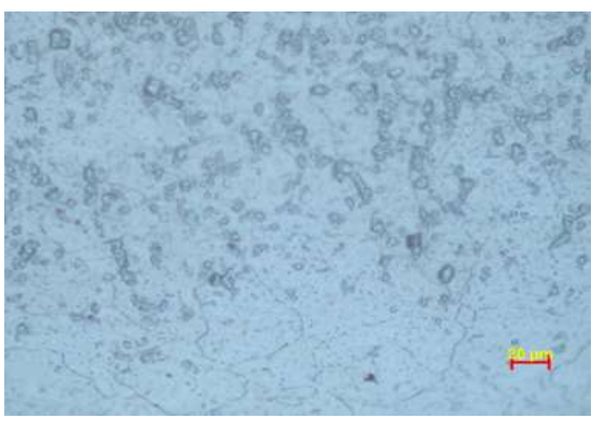

Figure 9 Microstructure at 500x of the AA1100 aluminum plate produced by conventional rolling

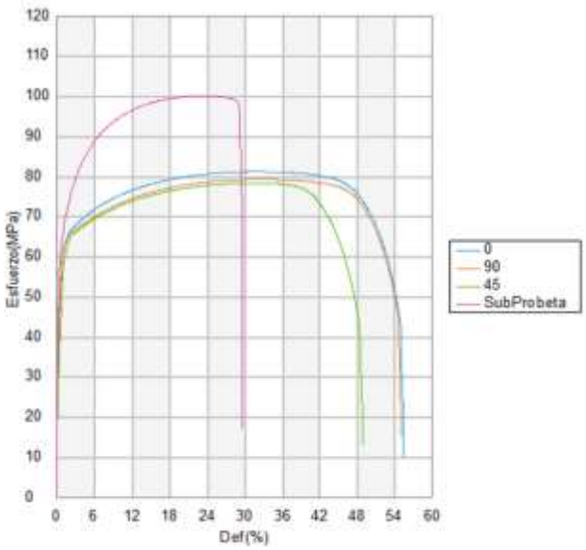

Graphic 1 Stress-strain curves of the aluminum plate(0°, 45 ° and 90° from the rolling direction) and the PM+HIP samples

Table 2 shows the average mechanical properties of the samples. There is seen that no big differences existed among the samples taken from the aluminum plate but there is a big differences between the mechanical properties taken from samples of the plate and the P/M+HIP samples.

	UTS (MPa)	Yield (MPa)	Lo (mm)	Lf (mm)	% Elong.
0	81.1135667	61.8447	50.00	81.16	62.32
45	78.0940333	61.4595	50.00	81.715	63.43
90	78.9505333	60.5781	50.00	81.0766667	62.15
P/M+HIP	100.024	59.3995	25.00	32.43	29.72

Table 2 Results of the mechanical properties measured using tensile test

Table 3 shows the impact toughness measured using Charpy impact test. There is a big difference between the between the absorbed energy of samples taken from the plate and the samples taken from the P/M+HIP.

Sample	Joules (average)
Plate 0° rolling direction	70.5
Plate 45° rolling direction	65.5
Plate 90° rolling direction	65.5
P/M+HIP	0.7

Table 3 Results of the impact toughness measured using Charpy impact test

ISSN-2531-2189

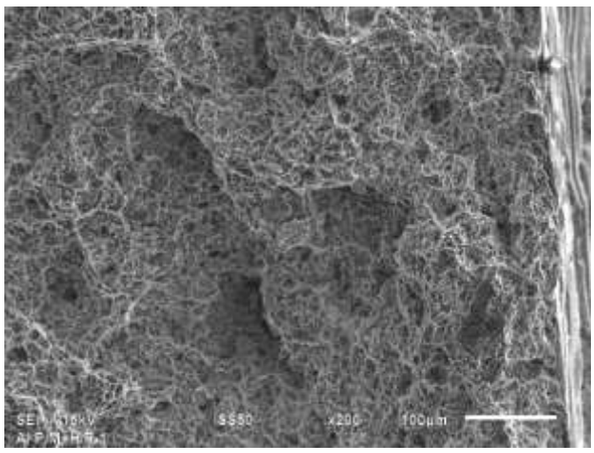

Figure 10 The SEM image shows the fracture Surface of the PM+HIP sample after Charpy testing

Figure 10 shows the fracture surface of the PM+HIP sample after tension testing. There is seen dimples, pores, and inclusions. Figure 11 shows the fracture surface of the PM+HIP sample after Charpy testing. There is seen dimples, pores, and inclusions.

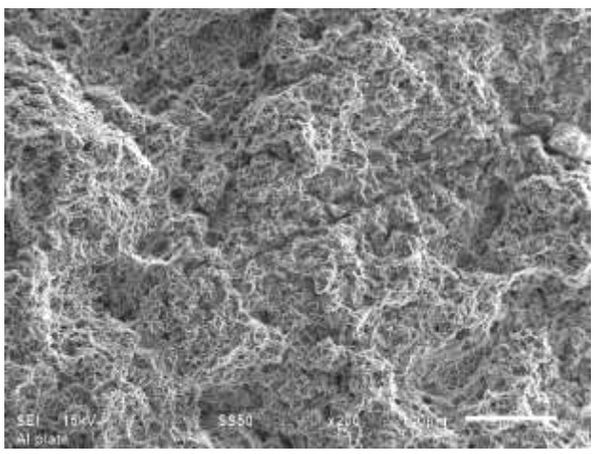

Figure 11 The SEM image shows the fracture Surface of the PM+HIP sample after tensile testing

Figure 12 shows the fracture surface of the plate with conventional rolling sample after Charpy testing.There is seen shearing dimples. Figure 13. The SEM image shows the fracture Surface of the plate with conventional rolling sample after tensile testing. There is seen tensile dimples.

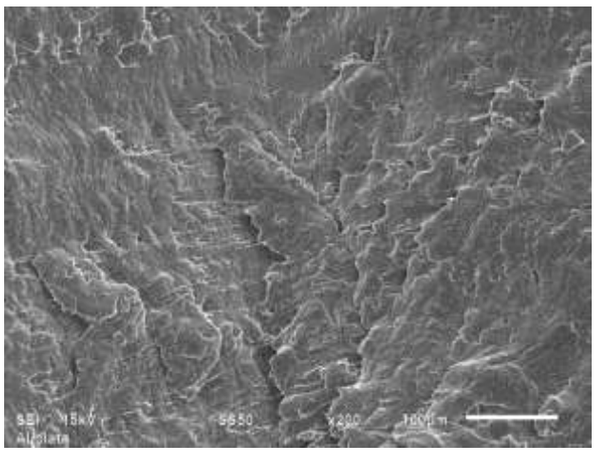

Figure 12 The SEM image shows the fracture Surface of the plate with conventional rolling sample after Charpy testing

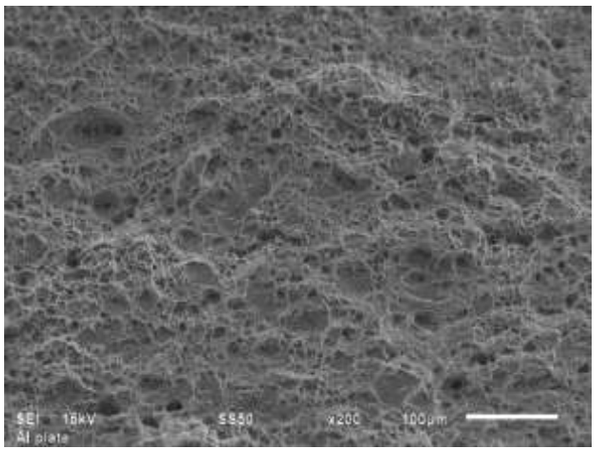

Figure 13 The SEM image shows the fracture Surface of the plate with conventional rolling sample after tensile testing

Discussion of results

The results of the chemical composition indicated that there is no big difference between the samples taken from the plate and the samples taken from the P/M+HIP. Both materials can be denominated as AA1100 aluminum. However, it must be kept in mind that the 1100 aluminum is almost pure aluminum but it is prone to strain hardening if it contains appreciable amounts of impurities such as iron and silicon. In the other hand, when this material is heated, the grain size might grow and the final grain size is influenced by impurities such as Cu, Fe, Mg, and Mn. In both cases there is an influence of the impurities in the microstructure and on the final mechanical properties of the material [1-3]. In this case the very low amount of impurities is an indication that no real influence of the impurities might be expected in the final mechanical properties of the aluminum billet P/M+ HIP.

ISSN-2531-2189

Nondestructive evaluation (NDE) techniques are utilized to look for internal porosity and establish control samples with known porosity size and distribution. In this case, the nondestructive inspection using X-ray microfocus CT cabinet system for 3D metrology and analysis model PHOENIX V/GTOME/XM was applied to the P/M+HIP aluminum billet. The results showed evidence of aligned and connected porosity in the interior of the P/M+HIP aluminum billet. This fact was important because the samples for mechanical testing were cut in different position of the porosity. Furthermore, it was interesting to find that the porosity was located near the external surface and in specific areas. This is clearly seen in figure 7. This fact matched with the information reported in literature, which stated that the skill of a HIP cycle to completely close all porosity in a material is dependent on the severity of the porosity and on the HIP parameters [12-14, 22, 23]. However, the evidences of the nondestructive inspection are indications of the effectiveness of HIP and the mechanical integrity. The last one is strongly influenced by the location and type of defects.

Figure 9 shows the typical microstructure of the AA1100 aluminum cold rolling plate, which consists of equiaxial grains of aluminum. There was observed no evidence of segregates. In the other hand, figure 8 shows the microstructure of the P/M+HIP billet, there is seen fine equiaxial grains with no evidences of porosity nor precipitates. However, the grain size of the aluminum plate is bigger than the one of the P/M+HIP billet. The differences in microstructures exhibited in the two aluminum samples processed by two different methods indicated a difference in mechanical properties. This statement was probed by the tensile tests and impact Charpy test.

The tensile mechanical properties showed that the yield strength of the aluminum plate and the P/M+HIP billet sample were very similar, around 60 MPa, which can be observed in table 1. It suggested that HIP has little effect on the yield strength. However, there was a relevant difference concerning the ultimate tensile strength (UTS) of both materials. The aluminum plate was 80 MPa in UTS, which is the reported tensile strength of this type of aluminum with no internal defects. Meanwhile, the P/M+HIP billet was around 100 MPa.

This difference is explained by the difference in grain sizes; if one keeps in mind the Hall-Petch relation between grain size and mechanical properties.

Contrary to the tensile mechanical properties, the impact toughness, measured using Charpy impact test, of the P/M+HIP billet was much lower than the one of the aluminum plate. This results confirm a brittle behavior of the P/M+HIP aluminum, which is opposite to the behavior of the aluminum plate. It is well known that impact toughness is influenced by many known factors. Not only is heat treatment a critical parameter, but also the amount of Sr, Fe, Mg, grain size, defects and microstructure [18-23]. In this case it is clear that only the grain size does not explains the low impact toughness but defects such as small voids or porosity does.

Even though P/M+HIP aluminum and the AA1100 aluminum cold rolling plate showed dimples in the fracture surfaces, they clearly indicated differences in crack growth between them. This probed by the presence of pores and inclusions on the fracture surface of the P/M+HIP aluminum, while there is no existence of such defects in the fracture surface of the AA1100 aluminum cold rolling plate. This fact indicates that defects played an important role in the crack growth.

Acknowledgments

The authors want to thank to Centro de Ingeniería y Desarrollo Industrial for the support during this work, to Eng. Maria Ofelia Wong for her support with the quantitative chemical analysis, to Dr. Diego German Espinosa for his help during the powder consolidation, MC. to Marco Antonio Paredes for his help with the nondestructive inspection using an X-ray microfocus CT cabinet system, and to MC. Alberto Gallardo for his support with the mechanical testing.

Conclusions

The previously discussed results led to the following conclusions.

It is possible to fabricate billets using P/M+HIP starting from aluminum powders but there is the existence of connected porosity, which has an effect in the mechanical integrity of the billet.

ISSN-2531-2189

This result was evident after the nondestructive inspection, which shows the need of nondestructive testing in component manufactured using P/M +HIP.

The tensile testing showed differences in properties between the P/M+HIP and the aluminum plate. The aluminum plate was 80 MPa in UTS, which is equivalent to the maximum material strength determined for sound material with no internal defects. Meanwhile, the P//M+HIP sample was around 100 MPa.

The impact toughness, measured using Charpy impact test, of the P/M+HIP billet was much lower than the one of the aluminum plate. This fact indicated a brittle behavior of the P/M +HIP material.

Defects such as pores or inclusions play an important role in the crack growth of P/M+HIP aluminum as it was seen in the fracture surfaces of the tensile and Charpy test samples.

References

[1] Davis, J. R. (1993). Aluminum and aluminum alloys. ASM international.

[2] MacKenzie, D. S., & Totten, G. E. (Eds.). (2003). Handbook of aluminum. New York: Dekker.

[3] Kaufman, J. G. (2000). Introduction to aluminum alloys and tempers. ASM international.

[4] Stein, J., Lenczowski, B., Fréty, N., & Anglaret, E. (2012). Mechanical reinforcement of a high-performance aluminium alloy AA5083 with homogeneously dispersed multi-walled carbon nanotubes. Carbon, 50(6), 2264-2272.

[5] Van Trinh, P., Van Luan, N., Phuong, D. D., Minh, P. N., Weibel, A., Mesguich, D., & Laurent, C. (2018). Microstructure, microhardness and thermal expansion of CNT/Al composites prepared by flake powder metallurgy. Composites Part A: Applied Science and Manufacturing, 105, 126-137.

[6] Agarwal, A., Bakshi, S. R., & Lahiri, D. (2016). Carbon nanotubes: reinforced metal matrix composites. CRC press.

[7] Richter, D., Haour, G., & Richon, D. (1985). Hot isostatic pressing (HIP). Materials & design, 6(6), 303-305.

[8] Manyanin, S. E., Vaxidov, Y. S., & Maslov, K. A. (2021, March). Theoretical aspects of production of products by hot isostatic pressing. In IOP conference series: materials science and engineering (Vol. 1079, No. 5, p. 052011). IOP Publishing.

[9] Bocanegra-Bernal, M. H. (2004). Hot isostatic pressing (HIP) technology and its applications to metals and ceramics. Journal of materials science, 39(21), 6399-6420.

[10] Buekenhout, L., & Alt, P. (1988). Hot isostatic pressing of metal powders. In Key Engineering Materials (Vol. 29, pp. 207-224). Trans Tech Publications Ltd.

[11] ASTM B998-17 "Standard Guide for Hot Isostatic Pressing (HIP) of Aluminum Alloy Castings". ASTM international. 2017.

[12] Billard, S., Fondère, J. P., Bacroix, B., & Dirras, G. F. (2006). Macroscopic and microscopic aspects of the deformation and fracture mechanisms of ultrafine-grained aluminum processed by hot isostatic pressing. Acta materialia, 54(2), 411-421.

[13] Gubicza, J., Dirras, G., Szommer, P., & Bacroix, B. (2007). Microstructure and yield strength of ultrafine grained aluminum processed by hot isostatic pressing. Materials Science and Engineering: A, 458(1-2), 385-390.

[14] Islam, M. A., & Farhat, Z. N. (2011). The influence of porosity and hot isostatic pressing treatment on wear characteristics of cast and P/M aluminum alloys. Wear, 271(9-10), 1594-1601.

[15] Dirras, G., Chauveau, T., Abdul-Latif, A., Gubicza, J., Ramtani, S., Bui, Q. & Bacroix, B. (2012). Ultrafine-grained aluminum processed by a combination of hot isostatic pressing and dynamic plastic deformation: microstructure and mechanical properties. Metallurgical and Materials Transactions A, 43, 1312-1322.

ISSN-2531-2189

[16] Almotairy, S. M., Boostani, A. F., Hassani, M., Wei, D., & Jiang, Z. Y. (2020). Effect of hot isostatic pressing on the mechanical properties of aluminium metal matrix nanocomposites produced by dual speed ball milling. Journal of Materials Research and Technology, 9(2), 1151-1161.

[17] Tjong, S. C., & Lau, K. C. (1999). Properties and abrasive wear of TiB2/Al-4% Cu composites produced by hot isostatic pressing. Composites Science and Technology, 59(13), 2005-2013.

[18] Lv, Y. Y., Zhang, L. F., Wang, G. X., & Xiong, Y. (2017, April). Effect of Rolling and Annealing on Microstructure and Mechanical Properties of High Purity Aluminum. In 3rd Annual International Conference on Advanced Material Engineering (AME 2017) (pp. 93-98). Atlantis Press.

[19] Tsepeleva, A., Novák, P., Kolesnichenko, E., Michalcová, A., Kačenka, Z., & Kubásek, J. (2022). Heat Treatment of Aluminum Alloys with the Natural Combination of Dopants. Materials, 15(16), 5541.

[20] Hung, C. H., Li, Y., Sutton, A., Chen, W. T., Gong, X., Pan, H., & Leu, M. C. (2020). Aluminum parts fabricated by laser-foil-printing additive manufacturing: processing, microstructure, and mechanical properties. Materials, 13(2), 414.

[21] Ashtiani, H. R. R., & Karami, P. (2015). Prediction of the microstructural variations of cold-worked pure aluminum during annealing process. Modeling and Numerical Simulation of Material Science, 5(01), 1.

[22] Du Plessis, A., & Macdonald, E. J. A. M. (2020). Hot isostatic pressing in metal additive manufacturing: X-ray tomography reveals details of pore closure. Additive Manufacturing, 34, 101191.

[23] Rich, T. P., Orbison, J. G., Duncan, R. S., Olivero, P. G., & Peterec, R. H. (1999). The effect of hot isostatic pressing on crack initiation, fatigue, and mechanical properties of two cast aluminum alloys. Journal of materials engineering and performance, 8, 315-324.

ISSN-2531-2189

[[Title in Times New Roman and Bold No. 14 in English and Spanish]

Surname (IN UPPERCASE), Name 1st Author†*, Surname (IN UPPERCASE), Name 1st Coauthor, Surname (IN UPPERCASE), Name 2nd Coauthor and Surname (IN UPPERCASE), Name 3rd Coauthor

Institutional Affiliation of Author including Dependency (No.10 Times New Roman and Italic)

International Identification of Science - Technology and Innovation

ID 1st Author: (ORC ID - Researcher ID Thomson, arXiv Author ID - PubMed Author ID - Open ID) and CVU 1st author: (Scholar-PNPC or SNI-CONAHCYT) (No.10 Times New Roman)

ID 1st Coauthor: (ORC ID - Researcher ID Thomson, arXiv Author ID - PubMed Author ID - Open ID) and CVU 1st coauthor: (Scholar or SNI) (No.10 Times New Roman)

ID 2nd Coauthor: (ORC ID - Researcher ID Thomson, arXiv Author ID - PubMed Author ID - Open ID) and CVU 2nd coauthor: (Scholar or SNI) (No.10 Times New Roman)

ID 3rd Coauthor: (ORC ID - Researcher ID Thomson, arXiv Author ID - PubMed Author ID - Open ID) and CVU 3rd coauthor: (Scholar or SNI) (No.10 Times New Roman)

(Report Submission Date: Month, Day, and Year); Accepted (Insert date of Acceptance: Use Only ECORFAN)

Abstract (In English, 150-200 words)

Objectives
Methodology
Contribution

Keywords (In English)

Indicate 3 keywords in Times New Roman and Bold No. 10

Abstract (In Spanish, 150-200 words)

Objectives
Methodology
Contribution

Keywords (In Spanish)

Indicate 3 keywords in Times New Roman and Bold No. 10

Citation: Surname (IN UPPERCASE), Name 1st Author, Surname (IN UPPERCASE), Name 1st Coauthor, Surname (IN UPPERCASE), Name 2nd Coauthor and Surname (IN UPPERCASE), Name 3rd Coauthor. Paper Title. Journal of Mechanical Engineering. Year 1-1: 1-11 [Times New Roman No.10]

* Correspondence to Author (example@example.org)
† Researcher contributing as first author.

Introduction

Text in Times New Roman No.12, single space.

General explanation of the subject and explain why it is important.

What is your added value with respect to other techniques?

Clearly focus each of its features

Clearly explain the problem to be solved and the central hypothesis.

Explanation of sections Article.

Development of headings and subheadings of the article with subsequent numbers

[Title No.12 in Times New Roman, single spaced and bold]

Products in development No.12 Times New Roman, single spaced.

Including graphs, figures and tables-Editable

In the article content any graphic, table and figure should be editable formats that can change size, type and number of letter, for the purposes of edition, these must be high quality, not pixelated and should be noticeable even reducing image scale.

[Indicating the title at the bottom with No.10 and Times New Roman Bold]

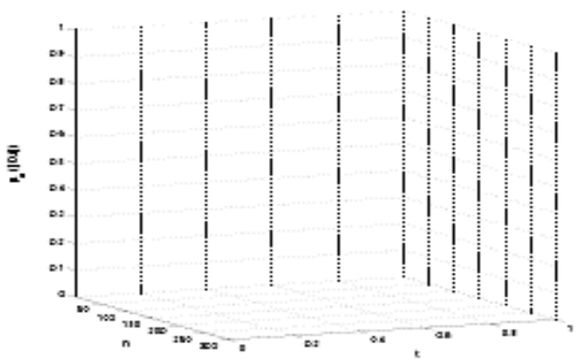

Graphic 1 Title and *Source (in italics)*

Should not be images-everything must be editable.

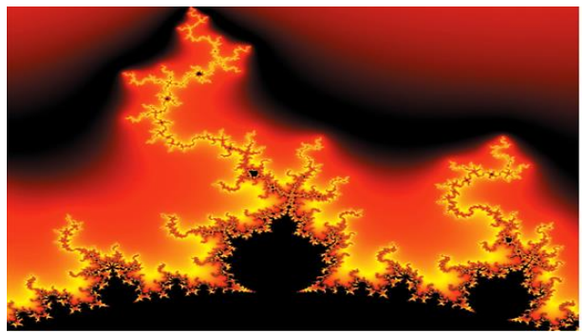

Figure 1 Title and *Source (in italics)*

Should not be images-everything must be editable.

Table 1 Title and *Source (in italics)*

Should not be images-everything must be editable.

Each article shall present separately in **3 folders**: a) Figures, b) Charts and c) Tables in .JPG format, indicating the number and sequential Bold Title.

For the use of equations, noted as follows:

$$Y_{ij} = \alpha + \sum_{h=1}^{r} \beta_h X_{hij} + u_j + e_{ij} \qquad (1)$$

Must be editable and number aligned on the right side.

Methodology

Develop give the meaning of the variables in linear writing and important is the comparison of the used criteria.

Results

The results shall be by section of the article.

Annexes

Tables and adequate sources

Acknowledgment

Indicate if they were financed by any institution, University or company.

ISSN 2531-2189

Conclusions

Explain clearly the results and possibilities of improvement.

References

Use APA system. Should not be numbered, nor with bullets, however if necessary numbering will be because reference or mention is made somewhere in the Article.

Use Roman Alphabet, all references you have used must be in the Roman Alphabet, even if you have quoted an Article, book in any of the official languages of the United Nations (English, French, German, Chinese, Russian, Portuguese, Italian, Spanish, Arabic), you must write the reference in Roman script and not in any of the official languages.

Technical Specifications

Each article must submit your dates into a Word document (.docx):

Journal Name
Article title
Abstract
Keywords
Article sections, for example:

1. Introduction
2. Description of the method
3. Analysis from the regression demand curve
4. Results
5. Thanks
6. Conclusions
7. References

Author Name (s)
Email Correspondence to Author
References

Intellectual Property Requirements for editing:

- Authentic Signature in Color of Originality Format Author and Coauthors.
- Authentic Signature in Color of the Acceptance Format of Author and Coauthors.
- Authentic Signature in blue color of the Conflict of Interest Format of Author and Co-authors.

ISSN 2531-2189

Reservation to Editorial Policy

Journal of Mechanical Engineering reserves the right to make editorial changes required to adapt the Articles to the Editorial Policy of the Journal. Once the Article is accepted in its final version, the Journal will send the author the proofs for review. ECORFAN® will only accept the correction of errata and errors or omissions arising from the editing process of the Journal, reserving in full the copyrights and content dissemination. No deletions, substitutions or additions that alter the formation of the Article will be accepted.

Code of Ethics - Good Practices and Declaration of Solution to Editorial Conflicts

Declaration of Originality and unpublished character of the Article, of Authors, on the obtaining of data and interpretation of results, Acknowledgments, Conflict of interests, Assignment of rights and Distribution.

The ECORFAN-Mexico, S.C. Management claims to Authors of Articles that its content must be original, unpublished and of Scientific, Technological and Innovation content to be submitted for evaluation.

The Authors signing the Article must be the same that have contributed to its conception, realization and development, as well as obtaining the data, interpreting the results, drafting and reviewing it. The Corresponding Author of the proposed Article will request the form that follows.

Article title:

– The sending of an Article to Journal of Mechanical Engineering emanates the commitment of the author not to submit it simultaneously to the consideration of other series publications for it must complement the Format of Originality for its Article, unless it is rejected by the Arbitration Committee, it may be withdrawn.

– None of the data presented in this article has been plagiarized or invented. The original data are clearly distinguished from those already published. And it is known of the test in PLAGSCAN if a level of plagiarism is detected Positive will not proceed to arbitrate.

– References are cited on which the information contained in the Article is based, as well as theories and data from other previously published Articles.

– The authors sign the Format of Authorization for their Article to be disseminated by means that ECORFAN-Mexico, S.C. In its Holding Spain considers pertinent for disclosure and diffusion of its Article its Rights of Work.

– Consent has been obtained from those who have contributed unpublished data obtained through verbal or written communication, and such communication and Authorship are adequately identified.

– The Author and Co-Authors who sign this work have participated in its planning, design and execution, as well as in the interpretation of the results. They also critically reviewed the paper, approved its final version and agreed with its publication.

– No signature responsible for the work has been omitted and the criteria of Scientific Authorization are satisfied.

– The results of this Article have been interpreted objectively. Any results contrary to the point of view of those who sign are exposed and discussed in the Article.

Copyright and Access

The publication of this Article supposes the transfer of the copyright to ECORFAN-Mexico, SC in its Holding Spain for its Journal of Mechanical Engineering, which reserves the right to distribute on the Web the published version of the Article and the making available of the Article in This format supposes for its Authors the fulfilment of what is established in the Law of Science and Technology of the United Mexican States, regarding the obligation to allow access to the results of Scientific Research.

Article Title:

Name and Surnames of the Contact Author and the Co-authors	Signature
1.	
2.	
3.	
4.	

Principles of Ethics and Declaration of Solution to Editorial Conflicts

Editor Responsibilities

The Publisher undertakes to guarantee the confidentiality of the evaluation process, it may not disclose to the Arbitrators the identity of the Authors, nor may it reveal the identity of the Arbitrators at any time.

The Editor assumes the responsibility to properly inform the Author of the stage of the editorial process in which the text is sent, as well as the resolutions of Double-Blind Review.

The Editor should evaluate manuscripts and their intellectual content without distinction of race, gender, sexual orientation, religious beliefs, ethnicity, nationality, or the political philosophy of the Authors.

The Editor and his editing team of ECORFAN® Holdings will not disclose any information about Articles submitted to anyone other than the corresponding Author.

The Editor should make fair and impartial decisions and ensure a fair Double-Blind Review.

Responsibilities of the Editorial Board

The description of the peer review processes is made known by the Editorial Board in order that the Authors know what the evaluation criteria are and will always be willing to justify any controversy in the evaluation process. In case of Plagiarism Detection to the Article the Committee notifies the Authors for Violation to the Right of Scientific, Technological and Innovation Authorization.

Responsibilities of the Arbitration Committee

The Arbitrators undertake to notify about any unethical conduct by the Authors and to indicate all the information that may be reason to reject the publication of the Articles. In addition, they must undertake to keep confidential information related to the Articles they evaluate.

Any manuscript received for your arbitration must be treated as confidential, should not be displayed or discussed with other experts, except with the permission of the Editor.

The Arbitrators must be conducted objectively, any personal criticism of the Author is inappropriate.

The Arbitrators must express their points of view with clarity and with valid arguments that contribute to the Scientific, Technological and Innovation of the Author.

The Arbitrators should not evaluate manuscripts in which they have conflicts of interest and have been notified to the Editor before submitting the Article for Double-Blind Review.

Responsibilities of the Authors

Authors must guarantee that their articles are the product of their original work and that the data has been obtained ethically.

Authors must ensure that they have not been previously published or that they are not considered in another serial publication.

Authors must strictly follow the rules for the publication of Defined Articles by the Editorial Board.

The authors have requested that the text in all its forms be an unethical editorial behavior and is unacceptable, consequently, any manuscript that incurs in plagiarism is eliminated and not considered for publication.

Authors should cite publications that have been influential in the nature of the Article submitted to arbitration.

Information services

Indexation - Bases and Repositories

LATINDEX (Scientific Journals of Latin America, Spain and Portugal)
RESEARCH GATE (Germany)
GOOGLE SCHOLAR (Citation indices-Google)
REDIB (Ibero-American Network of Innovation and Scientific Knowledge- CSIC)
MENDELEY (Bibliographic References Manager)
HISPANA (Information and Bibliographic Orientation-Spain)
UNIVERSIA (University Library-Madrid)

Publishing Services

Citation and Index Identification H
Management of Originality Format and Authorization
Testing Article with PLAGSCAN
Article Evaluation
Certificate of Double-Blind Review
Article Edition
Web layout
Indexing and Repository
ArticleTranslation
Article Publication
Certificate of Article
Service Billing

Editorial Policy and Management

38 Matacerquillas, CP-28411. Moralzarzal –Madrid-España. Phones: +52 1 55 6159 2296, +52 1 55 1260 0355, +52 1 55 6034 9181; Email: contact@ecorfan.org www.ecorfan.org

Journal of Mechanical Engineering

2531-2189
ISSN 2531-2189
www.ecorfan.org